Entanglement Phase Transition of Interacting Bosons under Random Measurements

A Thesis

submitted to
Indian Institute of Science Education and Research Pune
in partial fulfillment of the requirements for the
BS-MS Dual Degree Program

by

Sakshi Velvankar

Indian Institute of Science Education and Research Pune
Dr. Homi Bhabha Road,
Pashan, Pune 411008, INDIA.

May, 2024

Supervisor: Dr. Sumilan Banerjee
Indian Institute of Science, Banglore

Certificate

This is to certify that this dissertation entitled "Entanglement Phase Transition of Interacting Bosons under Random Measurements " towards the partial fulfilment of the BS-MS dual degree programme at the Indian Institute of Science Education and Research, Pune represents the study/work carried out by Sakshi Velvankar at Indian Institute of Science, Banglore under the supervision of Dr. Sumilan Banerjee, Associate Professor, Department of Physics, during the academic year 2023-2024.

Dr. Sumilan Banerjee

Committee:
Dr. Sumilan Banerjee
Prof. Deepak Dhar

Declaration

I hereby declare that the matter embodied in the report entitled " Entanglement Phase Transition of Interacting Bosons under Random Measurements", are the results of the work carried out by me at the Department of Physics, Indian Institute of Science, under the supervision of Dr. Sumilan Banerjee and the same has not been submitted elsewhere for any other degree.

Sakshi Velvankar

Acknowledgments

First and foremost I would like to thank my Supervisor, Dr. Sumilan Banerjee. His guidance has been instrumental in shaping my academic journey. I am also thankful to the students in Dr. Banerjee's group, especially Lokesh. Discussions with him and Sir always helped me.

I am also grateful to Prof. Deepak Dhar for evaluating my thesis and inspiring me with his words on my monthly reports to him.

My friends Vishal and Suyash were always with me at Google meetings, where we worked and laughed together. They made it easier to deal with the journey that is MS thesis by always encouraging me.

Also, I would like to thank Mummy, Baba, my entire family and all my friends for always believing in me and giving their unwavering support through my little life's ups and downs.

Abstract

In this thesis, we study the entanglement phase transition from volume-law to area-law entanglement in a hard-core boson chain model under continuous measurement of local occupation number. We are specifically interested in observing the effects of spatially random measurement strengths on this phase transition. We have used the quantum trajectory approach to model the measurement process. The random measurement strengths case is compared with the constant strengths case. Quantities like von Neumann Entanglement Entropy, particle densities, bipartite and tripartite mutual information, probability distribution of single site von Neumann entropy and connected correlation function of number operators are studied to get a more comprehensive look at the system under measurement. Finally, we perform the finite size scaling analysis to study scaling behaviours of entanglement entropy, bipartite mutual information and connected correlation function at the entanglement transitions. For random measurements on a purely hard-core boson chain, which can be mapped to a non-interacting model of fermions, we see entanglement entropy increasing linearly with system size for small mean values of the random strengths. The increase is suppressed for larger mean values. This suggests a possible entanglement transition, which also shows a maximum at the transition point in bipartite mutual information. We also observe significant changes in some quantities with increasing the variance of the distribution from which strengths are chosen. For interacting boson chain with the available results, we observe an increase in entanglement entropy with system size. From scaling analysis of the random case, we obtain exponents that are different from the constant case.

Contents

List of Figures

List of Tables

1

Introduction

The physics of quantum systems interacting with the external environment [9] [24] plays an important role in the foundational understanding of quantum mechanics[3]. The environment behaves as a measurement apparatus, conducting measurements on the quantum systems.

Measurement Induced Phase Transition (MIPT) is one of the fascinating phenomena present in the quantum realm. It occurs when a drastic discontinuous change takes place in the entanglement properties of a quantum system because of repeated measurements. The competition of scrambling unitary dynamics and continuous local measurements gives rise to this measurement induced phase transition in entanglement from volume law to area law as measurement strength increases.

As found in some experimental work [13] [8] [2], when we try to realize the measurement dynamics physically, there will be spatially random noise in some aspects of the device. This noise appears as a static disorder in measurement strength for monitored quantum systems, which can significantly affect critical points and associated phases.

Previous works have studied MIPTs in real systems[10] and systems with unitary time evolution generated by random unitary circuits [5] [16] with constant measurement strengths. In the work done in [10], signatures of measurement induced criticality are found in hard-core boson chain undergoing continuous monitoring with constant measurement strength. In the paper [23], to study the noise in monitored systems,

random quantum circuits with spatially varying measurement rates (some qubits getting preferentially measured over others) have been studied. In this study it was found that under such varying measurements, the transition and phases change drastically, flowing to an infinite-randomness fixed point at the critical measurement strength. The nature of the critical point in this scenario is very different from the case of the constant measurement rate. The entanglement structures here behave unusually. At the critical measurement rate, the entanglement of the subsystem scales as $S \sim \sqrt{l}$ instead of $logl$ as observed usually for homogeneous measurements where l is the size of the subsystem and the dynamical critical exponent becomes $z = \infty$. Griffiths phases where rare-region effects dominate certain quantities are present around the critical point. More details are provided in the chapter on random measurements.

Considering the above cases a natural question arises as to whether a measurement induced criticality occurs in quantum many-body systems that are relevant to realistic physical setups with random noise in some aspect of measurement. If such a transition even happens will there be any difference in the nature of its critical point as found in the random circuits? Motivated by this in the thesis, we have studied the hard-core boson chain Hamiltonian with randomness in the value of measurement strengths at each site.

The thesis has the following structure:

Chapter 2 discusses the Measurement Induced Phase Transition (MIPT) model in detail. We introduce quantum entanglement, quantum measurements and how continuous measurements are obtained. Further, we talk about quantum dynamics under continuous measurements and also present the numerical methodology to implement this dynamics. In the appendix of Chapter 2, we show the Runge-Kutta fourth-order method to perform the time evolution.

In chapter 3, we introduce the hard-core boson chain model on which we study the dynamics under continuous measurement of local occupation number. Here, we perform measurements with constant measurement strengths at all sites. We also introduce quantities like von Neumann Entanglement Entropy, particle densities, bipartite and tripartite mutual information, probability distribution of single site von Neumann entropy and connected correlation function of number operators to study the behaviour of the system under measurement in more detail. In the appendix of

this chapter, we discuss how to construct a Hamiltonian matrix and calculate bipartite mutual information using Python coding.

In Chapter 4, we study the effect of measurements with random strengths at each site, selected from two different distributions on the hard-core boson chain and compare them with the constant strengths case in Chapter 3. We also use the quantities described in Chapter 3 to study this case. For one of the distributions, we study the interacting chain under measurement.

In Chapter 5, the finite scaling size for the results of Chapters 3 and 4 is done and compared to get a better picture of the measurement induced phase transition.

Finally, in Chapter 6 we give an outlook and discuss future research possibilities that we can address further.

2

Measurement Induced Phase Transition

To understand measurement induced phase transition we have to first get familiarised with the concepts of quantum entanglement and entanglement entropy.

2.1. Quantum Entanglement

Quantum entanglement is a phenomenon that takes place when many-body quantum state is such that each particle's quantum state cannot be described independently of the state of the other, even when a large distance separates the particles.

Suppose there are two quantum systems Q and R with states $|\psi\rangle_Q$ and $|\psi\rangle_R$ respectively. A quantum state $|\psi\rangle$ of a system including both Q and R is called entangled when it can not be expressed as a direct product of states $|\psi\rangle_Q$ and $|\psi\rangle_R$ i.e.,

$$|\psi\rangle \neq |\psi\rangle_Q \otimes |\psi\rangle_R \tag{2.1}$$

For example, take the Bell-pair state

$$|\psi\rangle = \frac{1}{\sqrt{2}}(|\uparrow\rangle_Q |\downarrow\rangle_R - |\downarrow\rangle_Q |\uparrow\rangle_R) \tag{2.2}$$

This state can not be represented as a direct product of $|\uparrow\rangle$ (spin up) and $|\downarrow\rangle$ (spin down). Measuring the spin of Q will immediately collapse the spin state of its entangled

partner R.

Quantum Entanglement captures true quantum correlations that lack any classical counterpart. Entanglement can also be used to characterize various quantum phases and their transitions. Quantum entanglement has been studied theoretically as well as measured experimentally.

2.2. Entanglement entropy

We focus on entanglement probes as the measurement induced transition is present in the averaged quantities that are nonlinear in the reduced density matrix conditional on measurement outcomes [23].

Entanglement entropy is a measure of uncertainty in determining the state of a subsystem of a system in a pure state $|\psi\rangle$. To calculate entanglement entropy we divide the system into two parts, subsystem A and subsystem B, as shown in the Fig. 2.1.

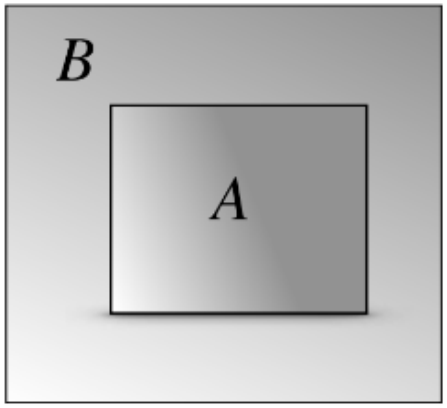

Figure 2.1: Bi-partition of a physical system in real space. Here, it is shown in 2D.

For a subsystem A, the von Neumann entanglement entropy is given by,

$$S_A = -Tr_A(\rho_A log \rho_A) \tag{2.3}$$

where,

The density matrix is,

$$\rho = |\psi\rangle \langle\psi| \tag{2.4}$$

and reduced density matrix for subsystems A is,

$$\rho_A = Tr_B \rho \tag{2.5}$$

where B is the rest of the system excluding A.

Below we describe the volume and area law of entanglement entropy.

Volume Law

For isolated systems exhibiting thermalization, bipartite entanglement entropy of an initially low entangled state, like a product state, grows linearly in time and after a long time saturates to a steady-state value. This value is in general, proportional to the volume of the subregion. This is called as the volume law of the entanglement entropy [10]. In systems obeying volume-law entanglement, extensively many degrees of freedom proportional to the volume of subsystem A are entangled with the exterior region.

Area law

In the systems following Area law, the entanglement entropy is proportional to the boundary or the surface area of the subsystem.

As shown in Fig. 2.2, showing area law, only the shaded boundary region proportional to ∂A contribute to the entanglement.

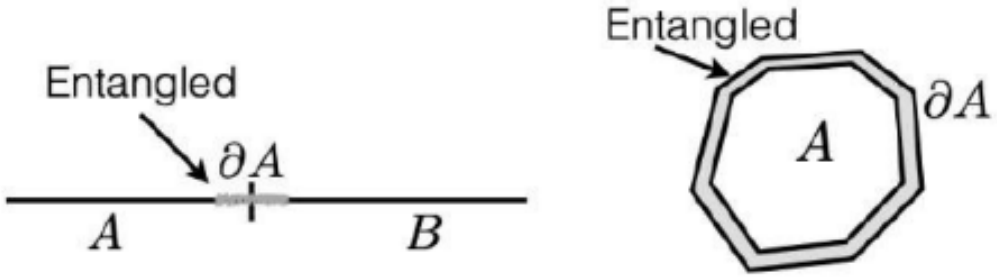

Figure 2.2: Area law entanglement entropy in one and two spatial dimensions. The figure is taken from ref. (2s)

2.3. MIPT

Entanglement is an important tool for understanding dynamics, nontrivial topology and critical phenomena of many-body quantum systems. Starting with an initial state with low entanglement, more entanglement is generated by unitary time evolutions

(determined by Hamiltonian or quantum gates) between two distant subregions of the system. On the other hand, the measurement of a local operator disentangles the measured local state from the rest of the system. As we do these measurements more and more it results in the decrease of entanglement entropy.

This competition between unitary dynamics and local quantum measurements gives rise to quantum phase transition in entanglement from volume law to area law as measurement strength is increased. The transition occurs at a particular critical value of measurement strength (p_c). MIPTs can also take place in the presence of measurement-only dynamics because of the competition between two non-commuting measurements as shown in the paper [11].

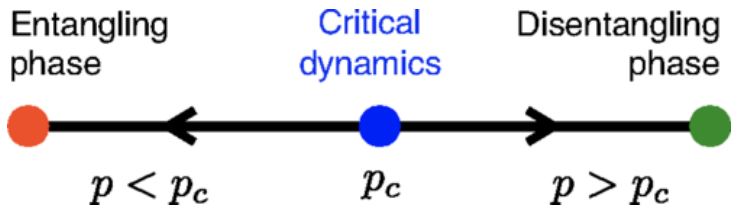

Figure 2.3: Measurement Induced Phase Transition from entangling volume law phase to disentangling area law phase as measurement strength p increases. The critical measurement strength is p_c. Figure taken from [19]

Unitary dynamics and measurements can be simulated using different models. We can use random unitary circuits and projective measurements as shown in Fig. 2.4. We can also use real physical systems with continuous quantum measurements.

As shown in Fig. 2.5, in the region with $p < p_c$ i.e., the entangling phase (upper curve), the entanglement growth is ballistic with time. Normally logarithmic growth is seen at the critical point p_c (middle curve). This is because of the scale invariance which also gives power-law correlations in connected correlation functions. In the $p > p_c$ disentangling region (lower curve), the entanglement saturates to a finite value.

2.4. Constructing Continuous Measurements

We are introduced to quantum measurement, which takes place without considering the time involved. The measurement just appears to happen instantaneously. However, this understanding of quantum measurements is incomplete.

Suppose we are continuously monitoring some observable of the system. Here,

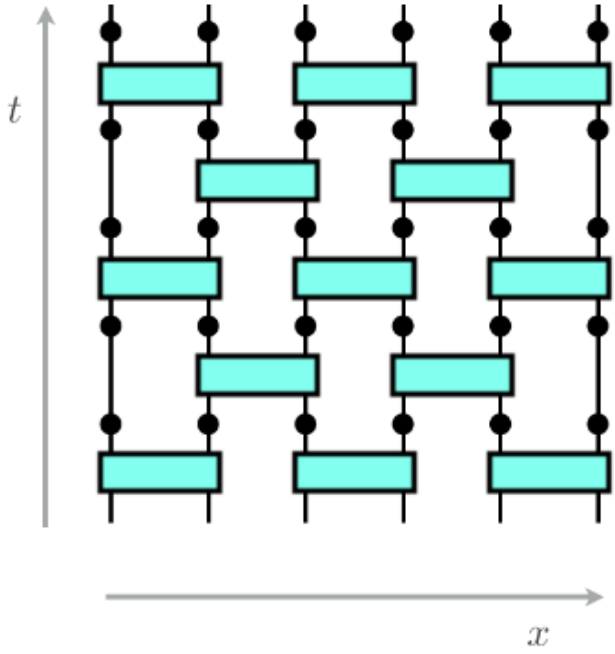

Figure 2.4: Circuits for the evolution of the quantum system. Unitary operators are shown by bricks and measurements can take place at dots showing spacetime locations. Figure taken from [19]

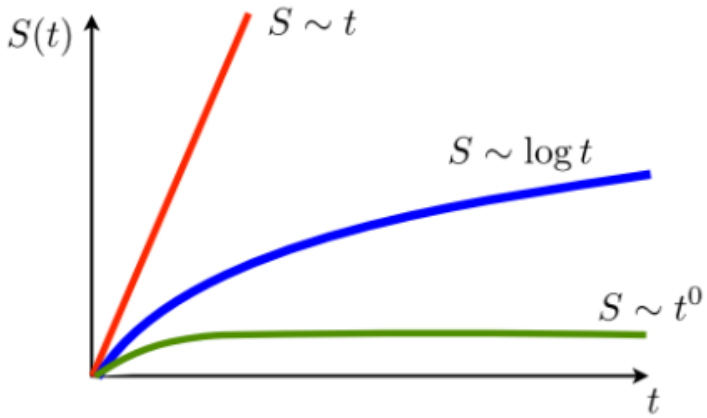

Figure 2.5: Bipartite entanglement entropy growth of an infinite chain for different values of measurement strengths. Figure taken from [19]

information is obtained at a finite rate and continuously so we need to understand what is happening to the system while the measurement is being done over it. Another point to consider is that nothing happens instantaneously. If the time of dynamics of the system is shorter or comparable to that of the measurement time then it is necessary to understand both the effect of measurement on the system and the dynamics of the flow of information to the observer[12]. Continuous quantum measurement describe such situations.

To understand Continuous Measurements we first need to understand projective, POVM and weak measurements.

POVMs and Weak measurements

We know von Neumann measurements. If the state of the system is $|\psi\rangle = \sum_n c_n |n\rangle$ where $|n\rangle$ with n=1,....n_{max} are the eigenstates, then the probability that system will be projected on $|n\rangle$ is $|c_n|^2$.

Complete information i.e. the exact value of the observable after the measurement is done is provided by von Neumann measurement.

There are measurements that give only partial information about the observable, meaning while it reduces the uncertainty of the observable, it is not completely removed.

The set of projection operators given below describes von Neumann measurements,

$$P_n = |n\rangle \langle n| \tag{2.6}$$

The initial state of the system can be given by the density operator $\rho = |\psi\rangle \langle \psi|$. The final state's nth possible outcome is then,

$$\rho_f = |n\rangle \langle n| = \frac{P_n \rho P_n}{Tr[P_n \rho P_n]} \tag{2.7}$$

the probability of getting this result is,

$$P(n) = Tr[P_n \rho P_n] = c_n \tag{2.8}$$

Using the same fashion we can make every possible measurement with N possible outcomes by generalizing the set of operators Ω_k with $\sum_{k=1}^{k_{max}} \Omega_k^\dagger \Omega_k = I$. I is the identity operator.

$$\rho_f = \frac{\Omega_k \rho \Omega_k^\dagger}{Tr[\Omega_k \rho \Omega_k^\dagger]} \tag{2.9}$$

with,

$$P(k) = Tr[\Omega_k \rho \Omega_k^\dagger] \tag{2.10}$$

is the probability of obtaining the kth outcome.

These generalised measurements are called POVMs (positive operator-valued measure). Thus the operater $K = \sum_{k=a}^{b} \Omega_k^\dagger \Omega_k$ gives the probability that k lies in the range $[a, b]$.

For measurements giving partial information, we choose Ω_k to be the weighted sum of projectors on the eigenstates instead of just simply projecting on a single eigenstate.

$$\Omega_k = \frac{1}{\mathcal{N}} \sum_n exp[-m(n-k)^2/4] \, |n\rangle \langle n| \tag{2.11}$$

Here $\mathcal{N}$ is the normalization constant.The final state after such a measurement is performed is,

$$\rho_f = \frac{\Omega_k \rho \Omega_k^\dagger}{Tr[\Omega_k \rho \Omega_k^\dagger]} = \frac{1}{\mathcal{N}} \sum_n exp[-m(n-k)^2/2] \, |n\rangle \langle n| \tag{2.12}$$

Here the final state is peaked at eigenvalue k and it has a width of $1/m^2$. As the value of m grows, the final uncertainty regarding the observable's value decreases. 'Strong measurements' are those which have a large value of m. 'Weak measurements' are conversely the measurements with small m. For constructing continuous measurements we will use these weak measurements.

Continuous Measurements

A measurement in which information is continually extracted from a system is called a continuous measurement [12]. This means that as the measurement duration goes to zero, the amount of information obtained will go to zero.

To construct continuous measurement, first divide time into a sequence of Δt length of intervals. In each interval consider a weak measurement. Next, we make the strength of each measurement proportional to the time interval and then take the limit in which the time intervals become infinitesimally small as $\Delta t \to 0$ (or similarly, $\Delta t \to dt$).

In this limit, in any finite time interval more and more measurements are done but each being increasingly weak. We choose the variance of the measurement result to scale to Δt, ensuring that a sensible continuum limit is obtained. Due to this random nature of the measurements we obtain a stochastic equation of motion. (A variable fluctuating randomly over time is a stochastic variable).

2.5. Quantum Dynamics Under Measurement

When a quantum system interacts with an external environment, the environment acts as a measurement apparatus, conducting measurements on the quantum system [21]. The environment provides random measurements, which are basically classical stochastic outcomes giving rise to stochastic quantum dynamics in quantum systems. [7]

Various methods are used to model the measurement process in quantum dynamical systems such as;

1) Quantum state diffusion (QSD): it is a continuous measurement protocol

2) Quantum jump process: here occasional abrupt measurement of the quantum system is done [17]

In this stochastic process, we obtain various quantum trajectories over which we can take averages later.

Quantum trajectory: A single quantum trajectory in a stochastic process is a specific sequence of measurements and their outcomes with the time evolutions between adjacent measurements. It can be shown as $|\psi(t, \xi_t)\rangle$, where ξ_t represents stochastic outcomes in the trajectory.

The averaged density matrix obtained from these quantum trajectories is,

$$\bar{\rho}(t)b = \overline{|\psi(t, \xi_t)\rangle \langle\psi(t, \xi_t)|} \tag{2.13}$$

here, $\overline{(...)}$ is the average over an ensemble of stochastic trajectories.

The $\bar{\rho}(t)$ follows Lindblad dynamics given by the Markovian master equation which describes unconditional, dissipative dynamics [6],

$$\frac{d\bar{\rho}(t)}{dt} = -i[H, \bar{\rho}(t)] + \sum_j \gamma_j (L_j \bar{\rho}(t) L_j^\dagger - \frac{1}{2} L_j^\dagger L_j \bar{\rho}(t) - \frac{1}{2} \bar{\rho}(t) L_j^\dagger L_j) \tag{2.14}$$

Here, H is the Hamiltonian of the system, L_j is the Lindblad operators (or jump operators) which shows the quantum measurement done on the system and γ_j is the strength of these measurements.

We can express this equation in the alternative form,

$$\frac{d\bar{\rho}(t)}{dt} = -i(H_{eff}\bar{\rho}(t) - \bar{\rho}(t)H_{eff}^{\dagger}) + \sum_j \gamma_j L_j \bar{\rho}(t) L_j^{\dagger} \tag{2.15}$$

Where,

$$H_{eff} = H - \frac{i}{2}\sum_j \gamma_j L_j^{\dagger} L_j \tag{2.16}$$

H_eff is called the effective Hamiltonian.

The Lindblad dynamics can be achieved by both QSD and quantum jump dynamics [6].

2.6. Quantum jump measurement process

In the quantum trajectory approach, measurements happen as quantum jumps associated with the non-Hermitian Hamiltonian's nonunitary time evolution.

We use the stochastic Schrodinger equation obeying the discrete stochastic process called as the marked point process for this modelling of quantum jump, [4] [10]

$$d\,|\psi(t)\rangle = -i\left(H_{eff} + \frac{i}{2}\sum_{j=1}^{L}\gamma_j ||L_j\,|\psi(t)\rangle\,||^2\right)|\psi(t)\rangle\,dt + \sum_{j=1}^{L}\left(\frac{L_j\,|\psi(t)\rangle}{||L_j\,|\psi(t)\rangle\,||} - |\psi(t)\rangle\right)d\xi_j(t) \tag{2.17}$$

$d\xi_j(t)$ are discrete random variables with the mean values,

$$E[d\xi_j(t)] = \gamma_j ||L_j\,|\psi(t)\rangle\,||^2 dt \tag{2.18}$$

here, $E[...]$ represents the average over the stochastic process. The stochastic calculus followed here is,

$$d\xi_j(t)d\xi_k(t) = \delta_{jk}d\xi_j(t) \tag{2.19}$$

Thus now we can evolve the quantum system but the effective non-Hermitian Hamiltonian given by,

$$H_{eff} = H - \frac{i}{2}\sum_{j=1}^{L}\gamma_j L_j^{\dagger} L_j \tag{2.20}$$

The time evolution by this non-Hermitian Hamiltonian is non-unitary. Let the time evolved state at time t be $|\psi(t)\rangle = e^{-iH_{eff}t}\,|\psi_0\rangle$, where $|\psi_0\rangle$ is the normalised initial state. Then $|\psi(t)\rangle$ is not normalised state meaning, $\langle\psi(t)|\psi(t)\rangle \neq 1$.

The normalised state will be given by,

$$\left|\bar{\psi}(t)\right\rangle = \frac{e^{-iH_{eff}t}\,|\psi_0\rangle}{||e^{-iH_{eff}t}\,|\psi_0\rangle\,||} \tag{2.21}$$

$e^{-iH_{eff}t}\,|\psi_0\rangle$ is the operator norm.

In the quantum jump techniques, the master equation is rewritten as a stochastic average over individual trajectories, which can be further evolved numerically in time as pure states. Using these techniques, the numerically heavy need to propagate a full-density matrix in time is avoided and this complex procedure is replaced with stochastic sampling. This stochastic sampling of states is beneficial as it requires the propagation of state vectors with size N_H only, where N_H is the dimension of Hilbert space. On the other hand, propagating the density matrix would have required us to deal with an object of size N_H^2. This makes it numerical efficient, though the downside is that we must collect many samples for small statistical errors. Also to maintain the efficiency in numerical calculations it is necessary that the number of samples needed remains smaller than the size of the Hilbert space. [6] Thus in the further analysis we will focus on the quantum trajectory approach to directly access the entanglement dynamics conditioned on measurement outcomes rather than the density matrices' unconditional dynamics by the Lindblad master equation.

2.7. Numerical Methodology

Here we describe the way to numerically simulate the measurement process i.e the update algorithm to simulate stochastic Schrodinger equation [10] [4]:

(1) First evolve the initial state $|\psi(0)\rangle$ starting from $t = 0$, by the Schrodinger equation with the non-Hermitian Hamiltonian H_{eff}

$$\frac{d\,|\psi(t)\rangle}{dt} = -iH_{eff}\,|\psi(t)\rangle \tag{2.22}$$

till waiting time t= τ selected by the following equation,

$$||e^{-iH_{eff}\tau}\,|\psi(t)\rangle\,||^2 = \eta \tag{2.23}$$

where η is a random number chosen from a uniform distribution in $[0, 1]$

(2) At $t = \tau$, make a quantum jump by the Lindblad operator L_j with the probability p_j given by,

$$p_j = \frac{\gamma_j||L_j\,|\psi(\tau)\rangle\,||^2}{\sum_k \gamma_k||L_k\,|\psi(\tau)\rangle\,||^2} \tag{2.24}$$

(3) Finally the state gets replaced as

$$|\psi(\tau)\rangle \rightarrow \frac{L_j\,|\psi(\tau)\rangle}{||L_j\,|\psi(\tau)\rangle\,||} \tag{2.25}$$

(4) We again start with step 1, now by replacing the initial state $|\psi(0)\rangle$ by Eq. 2.25. We keep repeating this process by choosing new random numbers till the maximum time chosen for calculations.

In this method, instead of performing the evolution for a fixed time length, the jumps occur at a certain point in time. Thus, both the time evolution under the effective Hamiltonian between the jumps and the times of these jumps can be solved numerically with arbitrary precision.

To perform this time evolution we have used the Runge-Kutta method which is explained in more detail in the appendix.

2.7.1. Choosing when to do measurement

We have Eq. 2.23 to decide the waiting time τ. To implement this in practical numerical calculations, the following way is used,

At the start of each iteration, we choose a random number η. Further in our calculation, we do the time propagation while the quantity, let's call it $Q = ||e^{-iH_{eff}\tau}\,|\psi(t)\rangle\,||^2$ is greater than that of η. When Q goes below η we stop and use the last propagated wave-function for further calculations i.e. for performing a quantum jump.

However, we have to improve this method more to get Q closer to that of η. Suppose the random number in one of the iterations is η=0.50. The wavefunction starts with giving the value of $||e^{-iH_{eff}\tau}\,|\psi(t)\rangle\,||^2$ as 1 at t=0 and with each step dt this value keeps

decreasing. Let's say at ndt the value is 0.56 and at $(n+1)dt$ it becomes 0.45, where n is some integer. If we used the wavefunctions at ndt or $(n+1)dt$ for measurement this can add error because of the significant difference between their corresponding Q and η.

Solution used:

Approximate what will be the time for the value to be η if at timendt and $(n+1)dt$ its values are 0.56 and 0.45 resp. Do this by linear interpolation. Say the time is T_r. Now select $dt_2 = (T_r - ndt)/d$ where, choose 'd' as required. The lesser the value of dt_2, the more the precision but also the running time will be more. Use this new dt_2 to now perform Runge-Kutta from ndt to T_r. This will give you a wavefunction at the end whose corresponding Q is closer to r. After the measurement of this wavefunction, from T_r repeat the unitary evolution with the original dt selecting new random number and repeat the above procedure with new dt_2 according to need.

2.7.2. Choosing where to do measurement

For performing step (2) given in the numerical Methodology we must select a particular Lindbland operator L_j to apply. This is done as explained below [6];

1) We have probabilities p_j between 0 and 1 such that $\sum_j p_j = 1$. Using this we make a list such as, $k_1 = p_1$, $k_2 = p_1 + p_2$, $k_3 = p_1 + p_2 + p_3$ and so on.

2)Next, we choose a second random number r_2, also from a uniform distribution in $[0, 1]$. We choose the first k_j which is greater than r_2 and thus the associated operator L_j is chosen to be applied.

A

Appendix

A.1. Numerical method for Time Evolution

The exact evolution of a wavefunction by a Hermitian Hamiltonian H is,

$$|\psi(t)\rangle = e^{-iHt}\,|\psi(0)\rangle \tag{A.1}$$

If a non-Hermitian Hamiltonian is taken and we want to evolve in discrete time we can not use exact evolution. As a solution to this, we have used the Rungge-Kutta order 4 (RK4) evolution method.

The Runge-Kutta evolution is [14],

$$y_{n+1} = y_n + \frac{1}{6}(k_1 + 2k_2 + 2k_3 + k_4) \tag{A.2}$$

where,

$$\begin{aligned} k_1 &= hf(x_n, y_n) \\ k_2 &= hf(x_n + \frac{h}{2}, y_n + \frac{1}{2}k_1) \\ k_3 &= hf(x_n + \frac{h}{2}, y_n + \frac{1}{2}k_2) \\ k_4 &= hf(x_n + h, y_n + k_3) \end{aligned}$$

First, we performed the unitary evolution dynamics without any measurement of the hard-core Bosons chain by evolving the Neel state by exact time evolution and runge-kutta evolution (RK4) of the Schrodinger equation in occupation number basis. This is done to benchmark RK4 method in further use while considering measurement.

In the Fig. A.1, we compared the RK4 evolution of Von Neumann entanglement entropy with the exact evolution Eq.A.1. We consider the initial state $|\psi(0)\rangle$ as $|10...10\rangle$.

By comparing Fig. A.2a and Fig. A.2b we can see how entropy calculated by RK4 method gets closer to exact as the time step decreases. But alongside this, the lower the value of dt, the more time will be taken in numerical evolution. Thus, for our analysis in this thesis, we have chosen the time-step to be $dt = 0.01$.

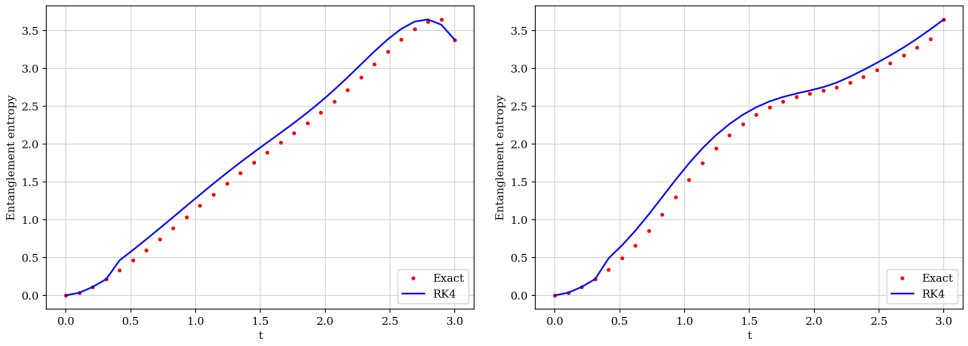

(a) V=0 **(b)** V=2

Figure A.1: Evolution of entanglement entropy in hard core boson chain with $L = 8, J' = 1, J = 1$ at half filling with only unitary evolution done by Exact evolution and RK4. Subsystem : (4,4), time-step=dt=0.1

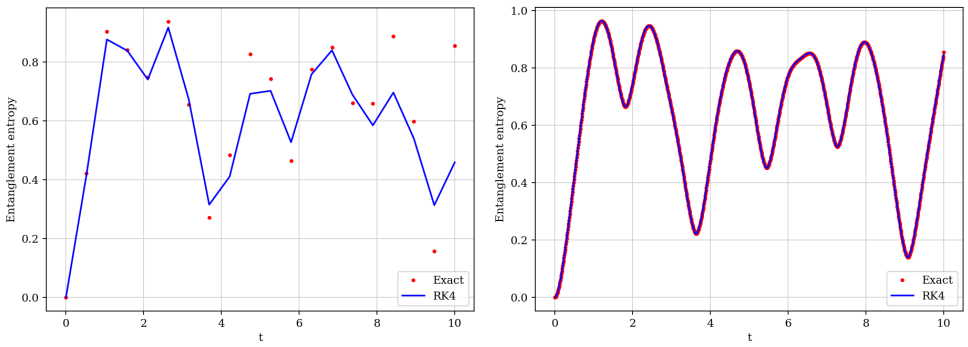

(a) time-step=0.5 **(b)** time-step=0.01

Figure A.2: Evolution of entanglement entropy in hard core boson chain with $L = 4, J' = 1, J = 1, V = 1$ at half filling with only unitary evolution . Subsystem : (2,2); As dt decrease the resemblance with exact evolution is more.

3

Measurement on hard-core boson chain

3.1. Model

We choose to study the behaviour of hard-core boson chain under continuous measurement of local particle numbers.

3.1.1. Hamiltonian of hard-core boson chain

The Hamiltonian of this model is,

$$H = \sum_{j=1}^{L} [\frac{J}{2}(b_j^\dagger b_{j+1} + b_{j+1}^\dagger b_j) + V n_j n_{j+1} + \frac{J'}{2}(b_j^\dagger b_{j+2} + b_{j+2}^\dagger b_j)] \tag{3.1}$$

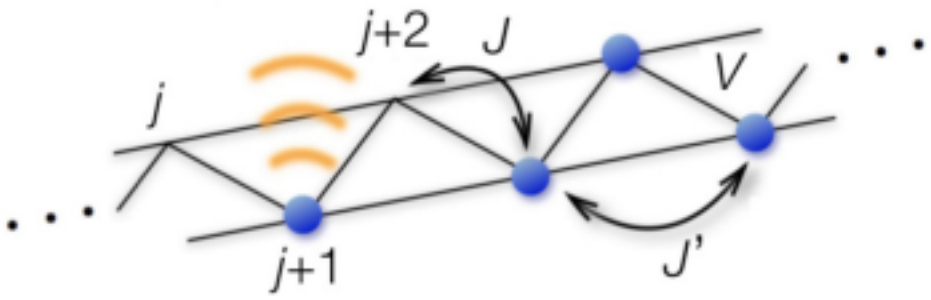

Figure 3.1: A hard-core boson chain with continuous measurement. Occupied sites are shown with blue circles and j is the label of the site. $J(J')$ is (next) nearest-neighbour hopping. V is interaction strength. Figure taken from [10]

L is the size of the system i.e. number of sites. J is the nearest neighbour hopping term and J' is the next nearest neighbour hopping term. V is the interaction strength. In all further analyses, we will keep $J = 1$ constant. b_j is the bosonic annihilation operator while $b_j^\dagger$ is the bosonic creation operator acting on site j. $n_j = b_j^\dagger b_j$ is the number operator. We place a hard-core constraint $(b_j)^2 = 0$, meaning each site can only be occupied by 0 or 1 boson. Throughout the thesis, we will consider periodic boundary conditions ($b_{L+j} = b_j$).

3.1.2. Dynamics under Continuous Measurement of local occupation number

We will now see the non-unitary dynamics of this 1D hard-core boson chain under continuous measurement using the quantum trajectory approach described in the previous chapter.

We choose to do the continuous measurement of local particle numbers in this model and thus can take the Lindblad operators to be,

$$L_j = n_j \tag{3.2}$$

We have, $n_j |N\rangle = N |N\rangle$ with hard core constraint (N=0 or 1 only). Thus for the number operator, we have the relation $n_j^2 = n_j$.

The dynamics of this model is then studied conditioned on measurement outcomes without averaging by focusing on the quantum trajectory of the pure state $|\psi(t)\rangle$. We use the stochastic Schrodinger equation obeying the discrete stochastic process called as the marked point process as described in Eq. 2.17

$$d|\psi(t)\rangle = -i\left(H_{eff} + \frac{i}{2}\sum_{j=1}^{L}\gamma_j||n_j|\psi(t)\rangle||^2\right)|\psi(t)\rangle\, dt + \sum_{j=1}^{L}\left(\frac{n_j|\psi(t)\rangle}{||n_j|\psi(t)\rangle||} - |\psi(t)\rangle\right)d\xi_j(t) \tag{3.3}$$

where H_{eff} is a non-Hermitian Hamiltonian,

$$H_{eff} = H - \frac{i}{2}\sum_{j=1}^{L}\gamma_j n_j n_j^\dagger \tag{3.4}$$

We will use the numerical procedure described in Chapter 2 to simulate the stochastic Schrodinger equation. By use of random number generators, we choose a time until which an initial state is evolved and then make a quantum jump at a site with a probability again chosen by random numbers [6].

We have the Eq. 2.23 to decide the waiting time to do the measurement. From this we get,

$$\begin{aligned} e^{-iH_{eff}\tau}e^{iH_{eff}^{\dagger}\tau} &= \eta \\ e^{-iH\tau}e^{\frac{i^2\tau}{2}\sum_{j=1}^{L}\gamma_j L_j L_j^{\dagger}}e^{iH\tau}e^{\frac{i^2\tau}{2}\sum_{j=1}^{L}\gamma_j L_j L_j^{\dagger}} &= \eta \\ e^{-\tau\sum_{j=1}^{L}\gamma_j L_j L_j^{\dagger}} &= \eta \end{aligned}$$

Thus,

$$\tau = \frac{-ln\eta}{\sum_{j=1}^{L}\gamma_j n_j n_j^{\dagger}} \tag{3.5}$$

with the relation $n_j^2 = n_j$ and $n_j^{\dagger} = n_j$, τ becomes,

$$\tau = \frac{-ln\eta}{\sum_{j=1}^{L}\gamma_j n_j} \tag{3.6}$$

3.2. Measurement with Constant measurement strengths

Here, let's consider a special case where the value of measurement strength at each site is the same,$\gamma_j = \gamma$ for all j. The non-Hermitian Hamiltonian with hard-core constraint then becomes,

$$H_{eff} = H - \gamma\frac{i}{2}\sum_{j=1}^{L} n_j \tag{3.7}$$

$$= H - \frac{iL\gamma\mathscr{D}}{2} \tag{3.8}$$

where $\mathscr{D} =< n_{tot} > /L$ is the filling of the initial state of the system. The total particle number $\sum_{j=1}^{L} n_j$ is conserved under time evolution by H_{eff} and measurements of n_j.

In all further analysis, we will consider a half-filled system, the initial state with fixed filling $\mathscr{D} = 1/2$ is then,

$$|\psi(0)\rangle = |0101...01\rangle \tag{3.9}$$

In this special case of constant measurement strengths on all lattice sites, the τ given by Eq. 3.6 becomes,

$$\tau = \frac{-ln\eta}{\gamma L \mathscr{D}} \tag{3.10}$$

Thus, because of the presence of constant measurement strengths and particle-number conservation, the non-Hermitian part of the Hamiltonian just becomes a constant and makes the frequency of observing quantum jumps to be the same.

We will now look into the system's entanglement probes described below. Along with this some other quantities are also given. In this chapter, the results of these quantities with only the constant measurement strengths are given. We will use the same quantities in further chapters to analyse measurement dynamics with random measurement strengths.

Note:

1. The RK4 method is used to perform the non-unitary time evolution, using a discrete-time dt. In our calculations, we majorly use $dt = 0.01$. We chose this value, as lower values of dt than this also gave the same convergence, but the process took more time.

2. As the trajectory proceeds we can calculate the quantities given below at each time step dt. To save time, but still get enough data set to take averages we calculate the quantities at each 50th step.

Any changes in the value of dt or step will be mentioned.

3.3. von Neumann Entanglement Entropy

To study entanglement properties and associated MIPTs in the steady state, we calculate the von Neumann Entanglement Entropy for subsystem A. For that, we first divide the system into two parts, subsystem A and subsystem B. The bi-partition of the Hilbert space of an N-body quantum system is $H_{AB} = H_A \otimes H_B$, where H is the Hilbert

space, $H_A(H_B)$ describes all the states in subsystems A and B respectively. In practical numerical calculations, we have obtained this Entropy by using the Singular Value Decomposition (SVD) method as follows.

Matrix decomposition means describing a given matrix by its constituent elements. All matrices have SVD.

$$A_{m\times n} = U_{m\times m}\sigma_{m\times n}V^T_{n\times n} \tag{3.11}$$

Where σ is a diagonal matrix, the diagonal values of this matrix are singular values of A.

Schmidt Decomposition of a state is given by;

$$|\psi\rangle = \sum_j \lambda_j |j\rangle_A |j\rangle_B \tag{3.12}$$

where $\lambda_j \in [0,1]$, $\sum_j \lambda_j^2 = 1$, $|j\rangle_A$ and $|j\rangle_B$ are orthonormal basis of the subspaces H_A and H_B respectively.

The density matrix is,

$$\begin{aligned}\rho &= |\psi\rangle\langle\psi| \\ &= \sum_j \sum_k \lambda_j\lambda_k |j\rangle_A |j\rangle_B \langle k|_A \langle k|_B\end{aligned}$$

Reduced density matrix for subsystems A and B,

$$\rho_A = Tr_B\rho = \sum_j \lambda_j^2 |j\rangle_A \langle j|_A \tag{3.13}$$

$$\rho_B = Tr_A\rho = \sum_j \lambda_j^2 |j\rangle_B \langle j|_B \tag{3.14}$$

Thus,

$$S_A = -Tr_A(\rho_A log\rho_A) = -\sum_j \lambda_j^2 log\lambda_j^2 \tag{3.15}$$

Entanglement Entropy is used to characterize the true quantum nature of various states. To characterize different phases or states, the system size scaling of this entropy is employed.

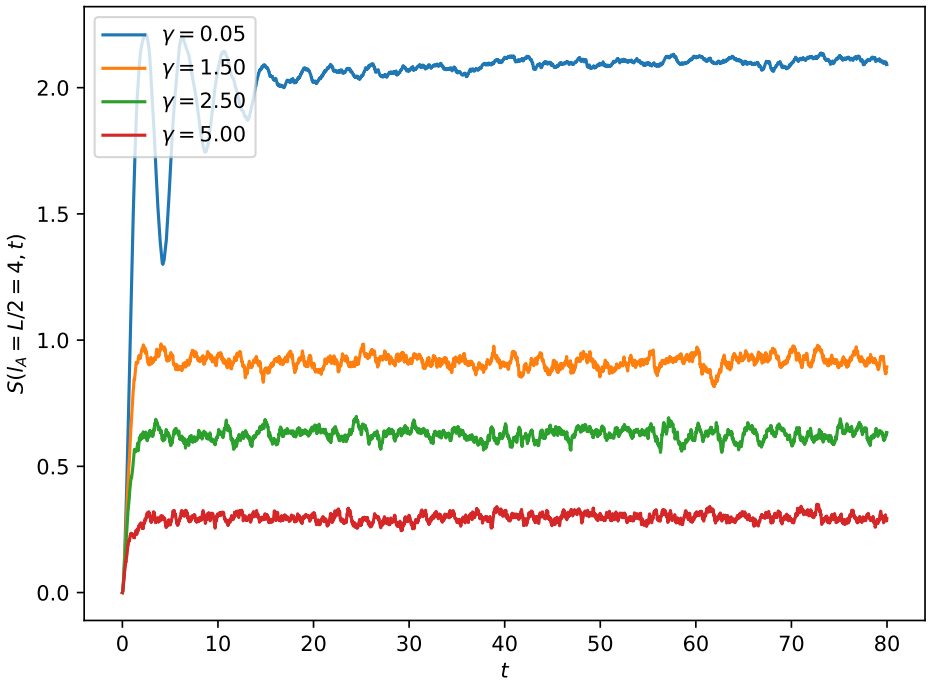

Figure 3.2: Entanglement Entropies of hard-core boson chain with $L = 8, J' = 1, J = 1, V = 0$ with half-filling averaged over 200 quantum trajectories for different values of γ. Here time step, $dt = 0.01$. The size of subsystem A is $L/2$.

3.4. Particle Densities

The particle density for a single quantum trajectory $|\psi(t)\rangle$ is,

$$< n_j(t) >= \langle\psi(t)|\, n_j \,|\psi(t)\rangle \tag{3.16}$$

As time progresses the particle density relaxes to the filling of about $\nu = 1/2$, Fig. 3.3b.

As shown in Fig. 3.3a, for a large value of measurement strength ($\gamma = 5$) more diffusive behaviour is observed in the density profile compared to a smaller value of strength ($\gamma = 0.5$).

This happens because of the competition between measurements and unitary time evolutions between successive measurements. The more the strength of measurement, the more the competition and more will be the diffusive behaviour.

We observe that the local occupation numbers quickly relax to a constant value in the interested timescale regime, thus making the probability distributions for measured positions of particles effectively uniform.

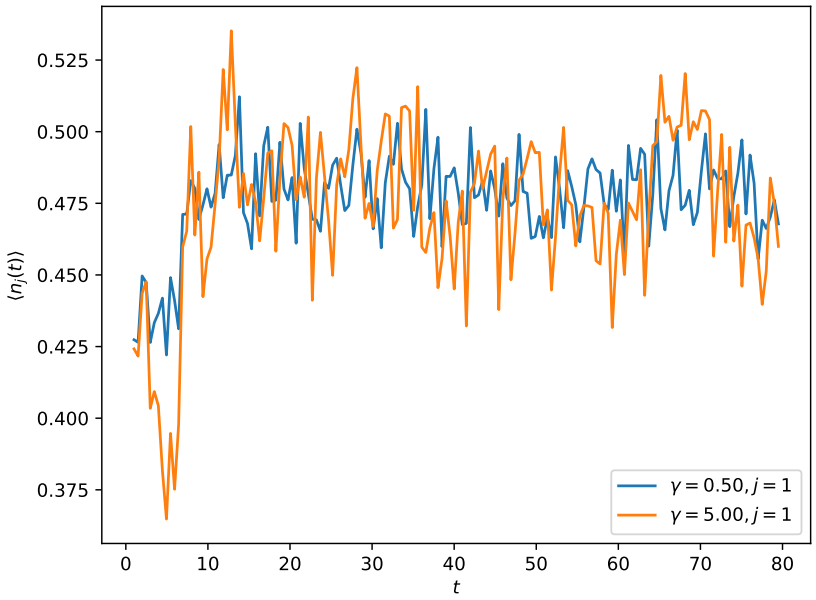

(a) Step=50

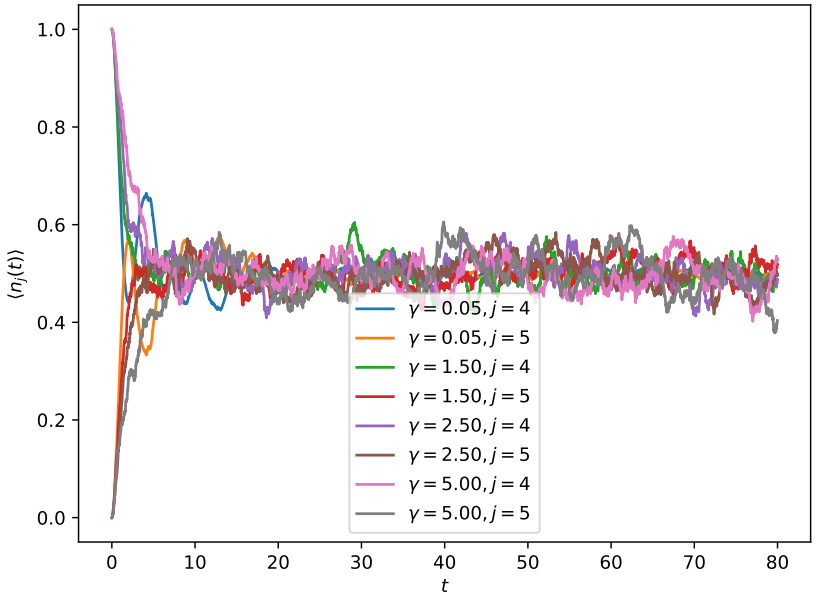

(b) Step=2

Figure 3.3: Local Particle densities of hard-core boson chain with $L = 8, J' = 1, J = 1, V = 0$ with half-filling

The particle-number fluctuation can be measured experimentally by site-resolved detection techniques which became possible due to quantum gas microscopy. [10]

3.5. Bipartite Mutual Information

Finding critical measurement strength γ_c by only fitting forms of small system sizes data of entanglement entropy is difficult. So, to quantify γ_c in a more convenient manner we study bipartite mutual information.

Quantum Mutual Information measures the correlation between subsystems of the quantum state.

Von-Neumann mutual information is defined as [10]

$$I_{AB}(t) = S_A(t) + S_B(t) - S_{A\cup B}(t) \tag{3.17}$$

where S_A and S_B are the von Neumann entanglement entropies of subsystems A and B embedded in the whole system, while $S_{A\cup B}$ is the entropy of their disjoint union.

We will take sub-regions A and B to be single sites which are separated by the distance r_{AB} on a ring of the length L. For all further analysis, the following values are used:

$A = \{1\}$

$B = \{r_{AB} + 1\}$

$A \cup B = \{1, r_{AB} + 1\}$

here $r_{AB} = L/2$

Mutual information in a steady-state regime has been observed to make a peak at the measurement-induced entanglement transition critical point with respect to measurement rate in some systems [10] [15] [22]. Different behaviours can be observed in different systems.

From Fig. 3.4a we can say that the critical strength of measurement-induced transition is near the vicinity of $\gamma = 1.4$. A more precise value of critical point can be obtained by considering higher system sizes.

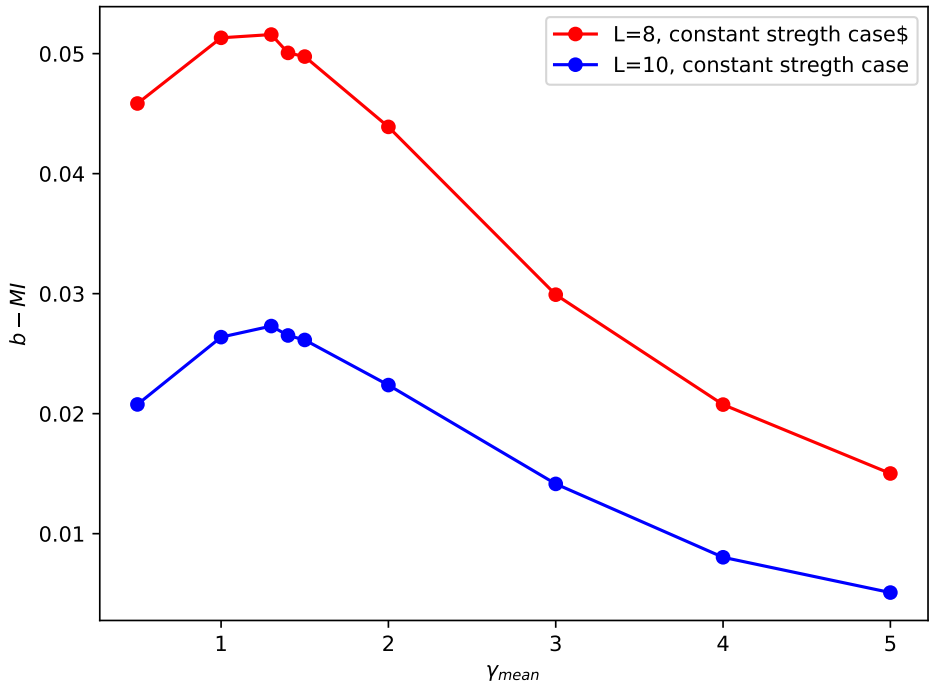

(a) Bipartite mutual information for L=8 and L=10 system sizes of hard-core boson chain with $J' = 1, J = 1, V = 0$ with half-filling (averages taken over time $t = 40$ to $t = 80$).

3.6. Tripartite Mutual Information

Tripartite Mutual information is defined as,

$$I_{ABC}(t) = S_A(t) + S_B(t) + S_C(t) - S_{A\cup B}(t) - S_{B\cup C}(t) - S_{A\cup C}(t) + S_{A\cup B\cup C}(t) \tag{3.18}$$

where A, B and C are sub-regions of the whole system.

In the paper [20], tripartite mutual information has extensive (negative) values in the volume-law phase. It is supposed to be finite at critical points with increasing system size and vanishing in the area law entangled states. The results can become more finer with increasing system size.

Thus, it is useful for determining the location of critical points as when we use its values for different system sizes it gives crossings with minimal finite-size drift.

Note that the result may not be the same for all kinds of systems.

In Fig. 3.5a we have shown the comparison of the values of tripartite mutual information with the same measurement strengths but considering different sub-regions A, B and C of single sites, but the distance between them varies. We can observe that as the measurement strength increases the difference between these two cases starts

decreasing.

In Fig. 3.5b the tripartite mutual information for two different system sizes is shown. As the strength of measurement increases, (typically in the area law regime) we observe that the value starts approaching zero. Also as the system size increases it is observed that in volume law region (smaller γ values) the values of tripartite mutual information become more negative.

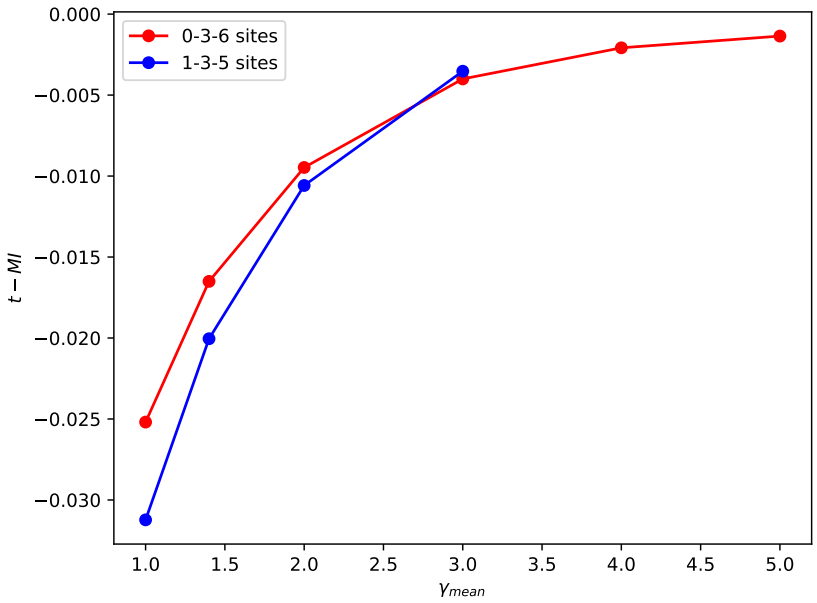

(a) Tripartite mutual information for different subregions of L=8 system.

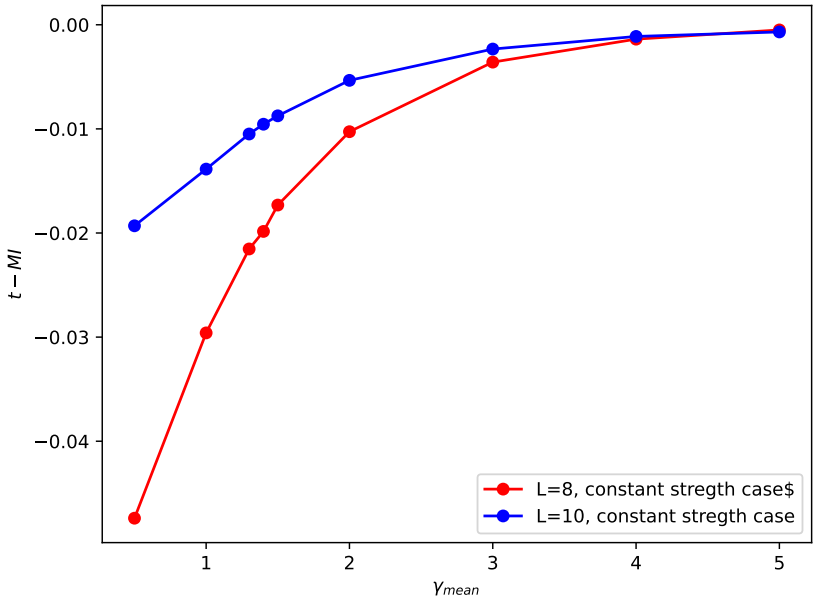

(b) Tripartite mutual information for system sizes L=8 and L=10.

3.7. Connected Correlation function

$$| < n_1 n_{L/2+1} >_c |^2 = | < n_1 n_{L/2+1} > - < n_1 >< n_{L/2+1} > |^2 \tag{3.19}$$

Here the first term is the expectation value of the product of operators and the second term is the product of their averages.

The expectation value of product factorises i.e. $< AB >=< A >< B >$ if A and B are statistically independent. Thus, $< ... >_c = 0$ if the degrees of freedom of X and X' are completely uncorrelated. Thus the γ at which this correlation function starts approaching zero we can say the system is becoming uncorrelated, its entanglement is getting lowered meaning it is the start of the Area-Law phase.

More precise values of γ_c will be obtained by taking larger system sizes.

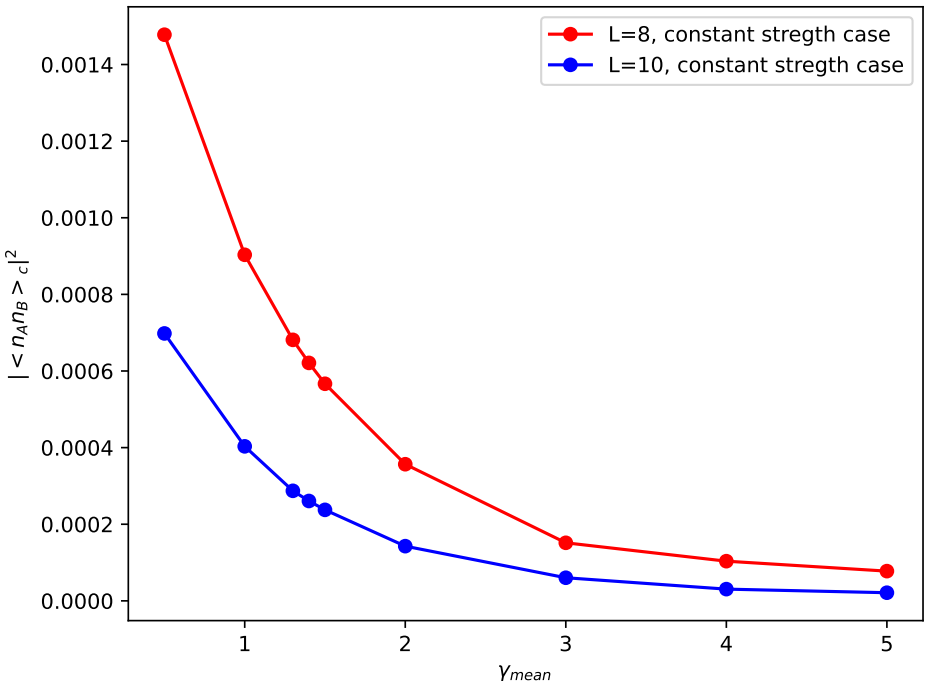

(a) Plot of $| < n_1 n_{L/2+1} >_c |^2$ for constant measurement strengths with J1=1, V=0 at L=8 and L=10 (averages taken over time t=40 to t=80).

3.8. Probability distribution of Single site Von Neumann entropy

Single-site Von Neumann entropy can be used as another indicator of the volume-to-area law transition in MIPTs. Site with j=1 is used to calculate this entropy, though all single

sites are equivalent as periodic boundary conditions are used.

Here in Fig. 3.7 and Fig. 3.8 we have plotted the probability distribution of Single-site Von Neumann entropy for different measurement strengths with $L = 8$ and constant measurement strength. The distributions are different in area and volume law phases.

In the volume-law phase with $\gamma = 0.5$ and 1 as shown in Fig.3.7b and 3.7c correspondingly, the single-site entropy distribution is seen to have two peaks. One is at $S = 0$ and the other at the end $S > 0$. If we consider pure unitary dynamics without any measurements, the local information should spread into the whole space, making the single site entanglement strong and thus only one peak should appear in the $S > 0$ side. But as measurements are present, they stabilize the quantum information, thus forming a peak near vanishing entropy [20].

As the area-law phase starts approaching with the increased strength of the measurement as in Fig. 3.8b and 3.8c, the peak at $S > 0$ starts disappearing and the peak at $S = 0$ starts becoming sharper. Deep in area law phase $\gamma = 5$ the sharpness is very prominent. The area law phase is a low entanglement phase.

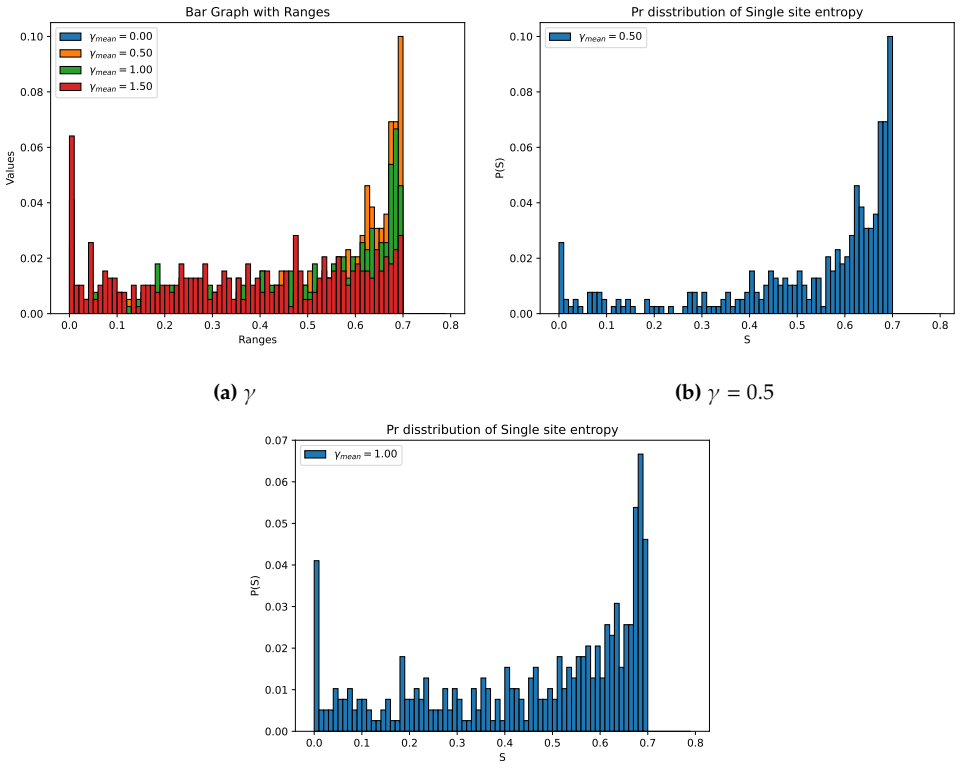

(a) γ

(b) $\gamma = 0.5$

(c) $\gamma = 1$

Figure 3.7

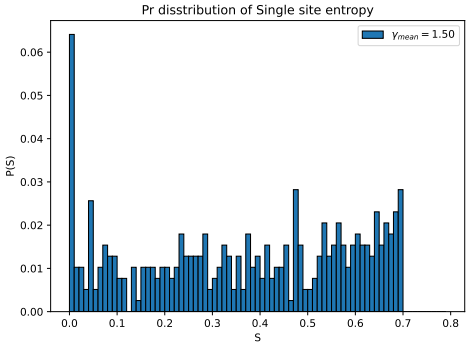

(a) $\gamma = 1.5$

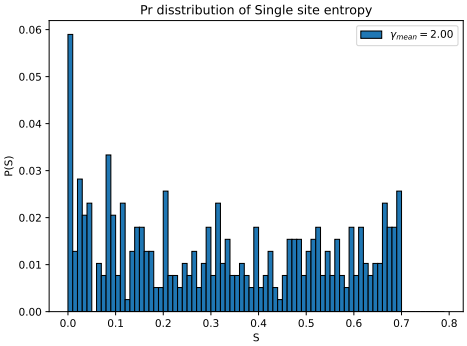

(b) $\gamma = 2$

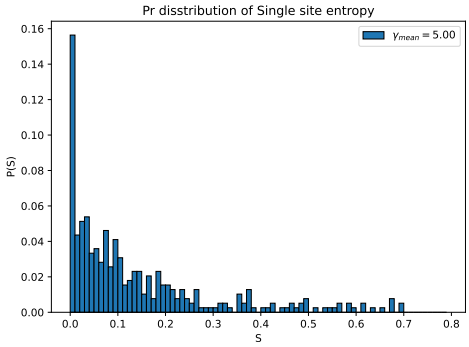

(c) $\gamma = 5$

Figure 3.8

B

Appendix

B.1. Constructing Hamiltonian

Considering periodic boundary conditions for $N = 4$ sites and 3 particles, the model becomes,

$$H = \frac{J}{2}(b_1^\dagger b_2 + b_1 b_2^\dagger) + V n_1 n_2 + \frac{J}{2}(b_2^\dagger b_3 + b_2 b_3^\dagger) + V n_2 n_3 + \frac{J}{2}(b_3^\dagger b_4 + b_3 b_4^\dagger) + V n_3 n_1 + \frac{J}{2}(b_4^\dagger b_1 + b_4 b_1^\dagger) + V n_4 n_1 \tag{B.1}$$

The basis states are $|0111\rangle$, $|1011\rangle$, $|1101\rangle$ and $|1110\rangle$.

$H|0111\rangle = \frac{J}{2}(|1011\rangle + |1110\rangle) + 2V|0111\rangle$ similarly, others can be found.

Thus, the Matrix becomes,

$$\begin{bmatrix} 2V & \frac{J}{2} & 0 & \frac{J}{2} \\ \frac{J}{2} & 2V & \frac{J}{2} & 0 \\ 0 & \frac{J}{2} & 2V & \frac{J}{2} \\ \frac{J}{2} & 0 & \frac{J}{2} & 2V \end{bmatrix}$$

Using such particle number conservation, we choose a basis such that the Hamiltonian (with all allowed particle numbers) becomes block-diagonal. Here, we use one such block, which can be diagonalized individually. This helps in doing more quicker numerical calculations of larger system sizes.

The simplest way is to enumerate the states and construct the Hamiltonian matrix using bits. We construct H by examining/flipping the bits. [1]

B.2. Calculating Bipartite Mutual Information (b-MI)

To calculate b-MI, we need to calculate entanglement entropy at site 1, site $(L/2+1)$ and their disjoint union. This is done in the following way,

Suppose we want to calculate S_A where A is the subsystem consisting of site 1, A={1}. Let the total system size be 8.

Usually in Python codes using SVD, the subsystem is partitioned at the end. Thus, we need to permute the site numbered 1 and 7. Sites are numbered as [0,7]. Only after this step can we perform the SVD.

The permutation is done as explained in the following example:

Let there be a system with 4 sites and 2 particles with a state,

$$|\psi_1\rangle = 0.5\,|1001\rangle + 0.5\,|0110\rangle \tag{B.2}$$

this is (0, 0, 0.5, 0.5, 0, 0, 0)

now, if we want to calculate S_A with A={2} we have to exchange site 2 and the last site 3, transforming the basis and thus the state as,

$$|\psi_1\rangle = 0.5\,|1010\rangle + 0.5\,|0101\rangle \tag{B.3}$$

this is (0, 0.5, 0, 0, 0.5, 0)

4

Hard-core Bosons under Random Measurement

In the previous chapter, we saw the behaviour of hard-core boson chain with spatially uniform measurement strengths at each site. From there we saw that there is a critical measurement strength below which the volume law phase of entanglement is present and above it, the area law phase is there. One can ask the question as to what happens if we take a random distribution of measurement strengths at each site. For example, will there be a sharp measurement-induced phase transition (MIPT)? If so, does the nature of the transition remain the same as the constant measurement case? Thus in this chapter, we will study the hard-core boson chain with continuous measurement of varying strength at each site of the chain. These varying strengths can be randomly chosen from a distribution and we will compare the mean values of measurement strength γ_{mean} obtained from these distributions with the values of γ from the previous chapter. Here we have studied two such distributions with varying means and variances.

As these distributions will contain values of γ both lower (for which previously volume-law phase was there) and higher (with the previous area-law phase), it is expected to show some different behaviour than that of the constant measurement strengths case. We expect to obtain significant changes by increasing the variance of the distribution for the same γ_{mean}.

Here the non-Hermitian Hamiltonian considered is,

$$H_{eff} = H - \frac{i}{2}\sum_{j=1}^{L}\gamma_j n_j \tag{4.1}$$

where H is the Hermitian Hamiltonian of hard-core boson chain Eq.3.1 and for one realization the values of measurement strengths at sites numbered with j, γ_j are selected from a particular distribution. The time evolution by this non-Hermitian Hamiltonian and modelling measurement process of local occupation number by quantum jump is performed as described in Chapter 2.

In practical numerical calculations first, we select a set of γ_j values from a certain distribution for $j = (0, L)$ sites. That particular set is kept constant and we run various quantum trajectories with this set. Further, we keep selecting other sets of γ_j values and their respective trajectories. Thus, we run (realizations × trajectories) runs in total. Higher values of the number of trajectories and realization can provide data with less statistical error.

Along with this, we will use the previously described indicators such as entanglement entropy, number-density, bipartite and tripartite mutual information, connected correlated function and single site entropy to study the transition from volume to area-law phase of entanglement.

4.1. Selecting Measurement Strengths from Uniform Distribution

In first case the values of γ_j at corresponding site j are randomly chosen from a uniform distribution of values between $[\gamma_{min}, \gamma_{max}]$ with mean $\gamma_{mean} = (\gamma_{max} + \gamma_{min})/2$ and variance $\Delta\gamma = (\gamma_{max} - \gamma_{min})/2$. We chose this kind of distribution to check the effect of increasing variances by keeping the mean constant on the measurement dynamics and associated transition.

4.1.1. Bench-marking the Random Measurement Strength Code

Here, we have performed the bench-marking of the code used for the random measurement strength case by comparing it with the results of Chapter 3. For performing bench-marking, in the random measurement strength code instead of generating a list

of random values of measurement, we have given a list of the same value repeated over sites for comparison with the previous code of constant measurement strengths. In the constant measurement case, τ is analytically obtained from Eq. 3.6, whereas in the random case, we need to obtain it by discrete evolution. We have compared bipartite mutual information Fig.4.1a and Connected correlation function Fig.4.1b. Data is taken for $L = 8, J' = 1, J = 1, V = 0$ with half-filling averaged over 400 quantum trajectories. Here $dt = 0.01$.

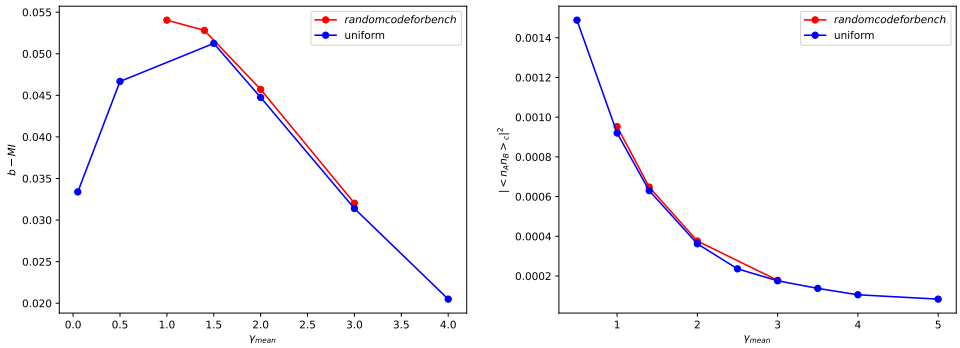

(a) bipartite Mutual information **(b)** connected correlation function

Figure 4.1: Bench-marking of Random measurement strength code

As the values from the two data sets are nearly similar for the same values of γ_{mean}, we can use this random measurement strength code for further calculations. The slight differences in the data points of the two sets could be because of the different sets of waiting times τ (as τ depends on the random number) that get generated in the time evolution of measurement dynamics, as described in Chapter 2. Lowering the value dt and increasing the number of trajectories can give better results as explained in previous chapters.

4.1.2. Results

In the following tables is the data obtained for averaged steady-state entanglement entropy with random measurements with different γ_{mean} chosen from uniform distributions with various $\Delta\gamma$ with $J' = J = 1, V = 0$ at half filling for different lengths.

From Tables 4.1 and 4.2, we observe that as the variance is increased the values of the steady state entanglement entropy for respective values of γ also increase. As seen in Table 4.3 more increase is observed for lower values of measurement strengths γ and it keeps steadily decreasing as the γ_{mean} increases. Also, a similar trend is observed as

γ_{mean} / $\Delta\gamma$	0	0.5	1
0.5	1.4848	1.5380	
1.5	0.8909	0.9206	0.9368
2.5	0.6075	0.6247	0.6331
5	0.2899	0.2976	0.2997
$L = 8, V = 0, J' = 1$			

Table 4.1: Values of steady state entanglement entropy for $L = 8$ length hard-core boson chain compared for different values of γ_{mean} and $\Delta\gamma$

γ_{mean} / $\Delta\gamma$	0	0.5
0.5	1.7886	1.8883
1.5	0.9707	1.0380
2.5	-	0.6790
5	0.2759	0.3128
$L = 10, V = 0, J' = 1$		

Table 4.2: Values of steady state entanglement entropy for $L = 10$ length hard-core boson chain compared for different values of γ_{mean} and $\Delta\gamma$

γ_{mean}	difference ($L = 8$)	difference ($L = 10$)
0.5	0.0532	0.0997
1.5	0.0162	0.0673
2.5	0.0084	-
5	0.0021	0.0369

Table 4.3: Difference between the values of steady state entanglement entropy (S) calculated as S($\Delta\gamma = 0.5$) - S($\Delta\gamma = 0$) compared for two different lengths (L).

we increase the length of the system though the values of differences become higher than their respective counterparts at lower lengths. This could be because the change due to disorder is effective when the mean and the variance are comparable. For higher values of measurement strengths, the same variance doesn't play much significant role.

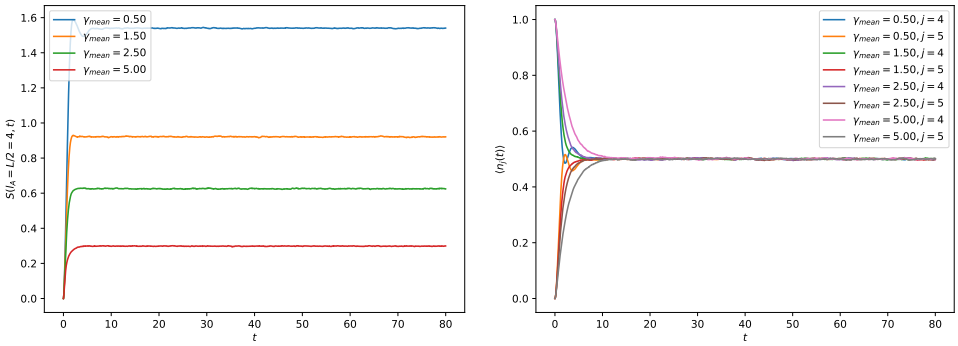

(a) Entanglement entropy **(b)** Average particle density

Figure 4.2: $L = 8, \Delta\gamma = 0.5$
180 trajectories, 300 realizations, $dt = 0.01$

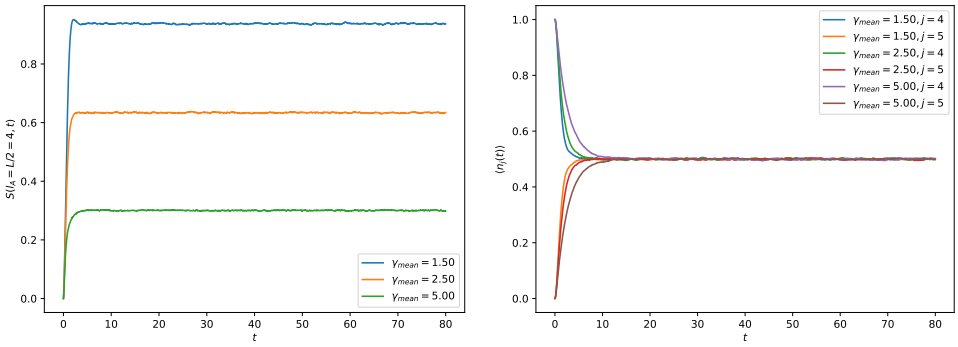

(a) Entanglement entropy **(b)** Average particle density

Figure 4.3: $L = 8$, $\Delta\gamma = 1$
180 trajectories, 300 realizations, $dt = 0.01$

In the figures 4.2, 4.3 and 4.4, we have shown the plots for entanglement entropy and number density for different values of γ_{mean}. We observe that for different values of length and variances, the number density settles down to 0.5 in a short amount of time. It takes a bit longer time to settle down to this density of 0.5 with increasing γ_{mean} values. The values are taken for sites $j = 4$ and $j = 5$ starting with the initial particle number of 1 and 0 respectively.

Along with this, these plots are smoother than the plots of the same quantities for constant measurement strengths in Chapter 3 (Fig. 3.2 and 3.3b). This is because these

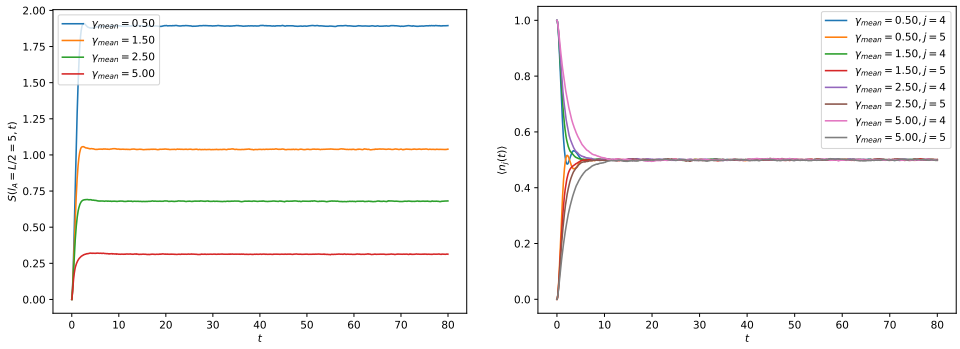

(a) Entanglement entropy **(b)** Average particle density

Figure 4.4: $L = 10$, $\Delta\gamma = 0.5$
400 trajectories, 200 realizations, $dt = 0.01$

values are averaged over more runs (trajectories × realizations) than those of constant case runs (trajectories).

4.1.3. Problem with constant Distribution of random values of strengths

As we keep increasing the variances $\Delta\gamma$ we can observe that the values of entanglement entropy are slightly increasing. To observe significant changes, we have to take larger variances, which will include negative values of the measurement strengths. However, as we can not take negative values of strengths we have to choose some other distribution for our analysis of random measurement strengths. If we take negative values of γ then the probabilities p_j of making quantum jumps as given by Eq. 2.24 can become negative which is not allowed.

4.2. Selecting Measurement Strengths from $\gamma_{max} r_i^n$ distribution

The paper on infinite-randomness criticality in monitored quantum dynamics with static disorder [23] uses a model of random quantum circuits with spatially varying measurement rates. A position-dependent measurement probability $p_x = r_x^n$ is applied. Here r_x is the random variable chosen from a uniform distribution between 0 and 1 and n is the tuning parameter. The strength of the measurement rate is parameterized by disorder averaged value and is $\bar{p} = 1/(n+1)$. This gives long tails and a columnar kind of distribution. This model addresses physical situations where some qubits are

preferentially measured over others.

The circuits described in the paper undergo a MIPT in the entanglement structure, though the nature of the critical point is very different from that of the constant measurement rate case. Using such a model the paper claims to obtain an infinite randomness critical point, where at the critical strength the Entanglement Entropy of a subsystem with size l scales as $\sqrt{l}$ instead of the normal $log(l)$ seen in homogeneous measurements. The dynamic critical exponent which gives information on how the characteristic timescale diverges near the critical point in the system is $z = \infty$. The transition point is surrounded by Griffiths phases with continuously varying dynamical exponents. Here certain dynamical quantities are dominated by the rare-region effects.

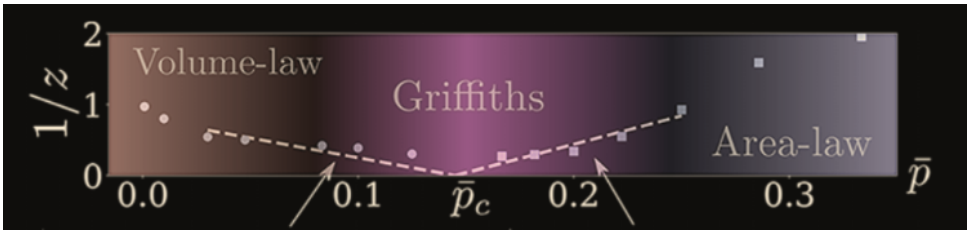

(a) The behaviour of the dynamic exponent z shown in the phase diagram of the disordered circuit model, near the Griffiths phases and the critical point. $\bar{p}$ is the average measurement rate. Figure taken from reference [23].

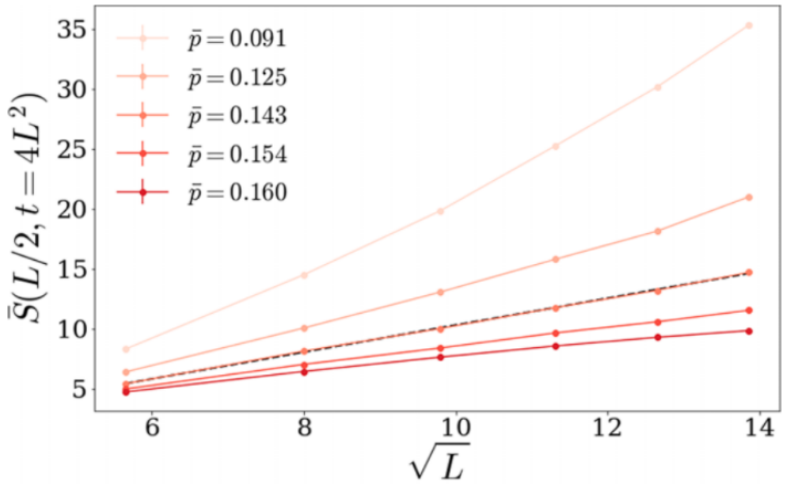

(a) Average half-cut entanglement entropy. Near the critical point, the entanglement entropy scales as $\bar{S} \sim \sqrt{L}$. Figure taken from reference [23].

We are trying to do a similar analysis on our model and see how the nature of the critical points and phases is affected.

For this, instead of position-dependent measurement probability, we take measurement strengths $p_i = \gamma_m r_i^n$ where again r_i is a random number from a uniform

distribution [0,1]. Here we will take $\gamma_m = 5$ and 10 and will scan over the range of n.

4.2.1. Probability distribution

For random variable $X_i = \gamma_m r_i^n$,

$$F(x) = P(X <= x) \tag{4.2}$$
$$= P(\gamma_m r_i^n < x) \tag{4.3}$$
$$= (x/\gamma_m)^{1/n} \tag{4.4}$$

Probability distribution function,

$$f(x) = F'(x) \tag{4.5}$$
$$= (x^{\frac{1}{n}-1})/(n\gamma_m^{\frac{1}{n}}) \tag{4.6}$$

Probability,

$$P(a < x < b) = \int_a^b f(x)dx \tag{4.7}$$
$$= (b^{\frac{1}{n}} - a^{\frac{1}{n}})/\gamma_m^{\frac{1}{n}} \tag{4.8}$$

Mean,

$$Mean = \int_0^{\gamma_m} x f(x)dx \tag{4.9}$$
$$= \gamma_m/(n+1) \tag{4.10}$$

Variance,

$$var = \frac{\gamma_m^2}{n+2} - (\frac{\gamma_m}{n+1})^2 \tag{4.11}$$

Below we have plotted the probability distribution and mean and variances for corresponding values of n and γ_{max}.

As shown in Fig.4.8 for same value of γ_{mean} variance increases as the value of γ_{max} is increased. Thus more changes are expected in the dynamics of distribution with higher γ_{max} when compared with that of the constant measurement strength case.

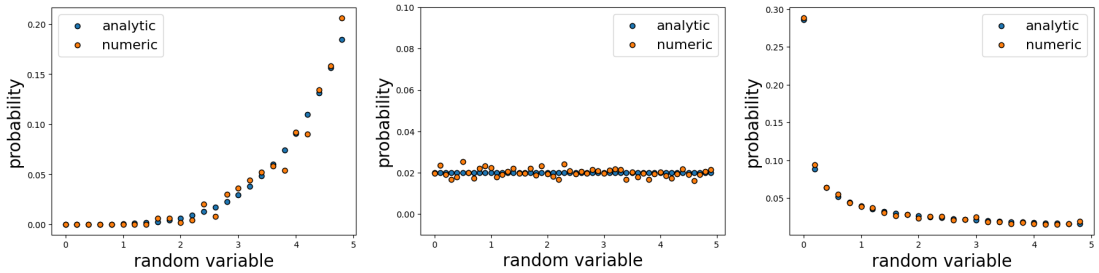

(a) $n = 0.2, \gamma_{max} = 5$ **(b)** $n = 1, \gamma_{max} = 5$ **(c)** $n = 2.5714, \gamma_{max} = 5$

Figure 4.7: probability distribution

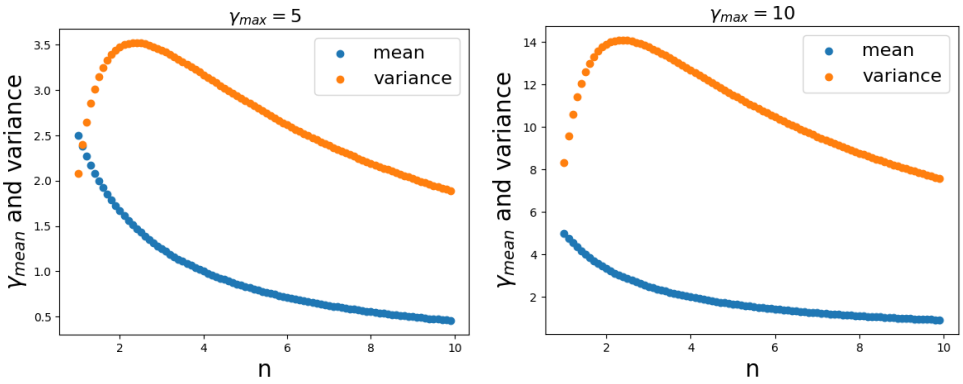

(a) Variance and mean for $\gamma_{max} = 5$ **(b)** Variance and mean for $\gamma_{max} = 10$

Figure 4.8: Comparison of mean and variances for different γ_{max} values.

For scanning over various values of γ_{mean} and variances we adjust over the values of n and γ_{max} accordingly.

4.2.2. Entanglement Profiles of non-interacting bosons chain

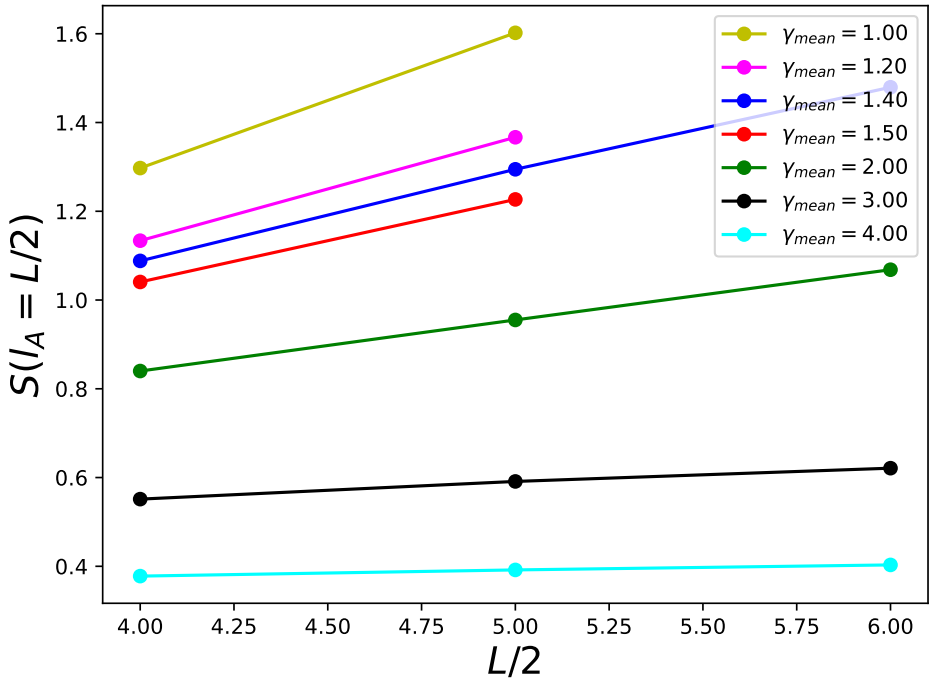

(a)

Figure 4.9: Steady-state values of von Neumann entanglement entropies with $V = 0, J' = 1, J = 1$ values, for different measurement strengths γ_{mean} for the distribution $\gamma_i = 5r_i^n$

Purely hard-core bosons with $V = 0$ in $1D$ can be mapped to the spin $1/2$ non-interacting fermions. We refer to this case as the *non-interacting* bosons in this thesis.

The steady-state entanglement entropies are obtained $S(l_A = L/2)$ are obtained by averaging $S(l_A, t)$ over time interval $[50, 100]$. In Fig.4.9 we have shown the system size dependence of half-chain entanglement entropies in the steady state regime. By this we observe that, for small γ_{mean} the entanglement entropy appears to increase linearly in the system, suggesting volume-law entanglement. This increase is suppressed for large γ_{mean} values, suggesting the area-law entanglement caused because of the frequent applications of the measurements. To see exactly if volume and area law phase are present, whether phase transition is happening and to check the scaling of entanglement entropy at entanglement transition (lnL or $\sqrt{L}$) we need to take larger system sizes and

more values of γ_{mean}.

4.2.3. Mutual information and correlation function for boson chain with $V = 0$

First, we study a non-interacting boson chain with V =0 with the continuous measurement of the local occupation number with random strengths. Here, $J1 = J = 1$ with half-filling.

The following data is for the system with lengths L with distributions $5r^n$ and $10r^n$. It is plotted with comparison to that of the constant distribution case where each site has the same measurement strength. The data is averaged over 400 trajectories and 200 realizations over time 50-80 and $dt = 0.01$. Entanglement entropy and other values are calculated at every $50th$ step.

For bipartite mutual information, we are using sites 1 and $L/2 + 1$ as mentioned in chapter 2.

For tripartite mutual information, we use sites numbered 1, 3, and 5.

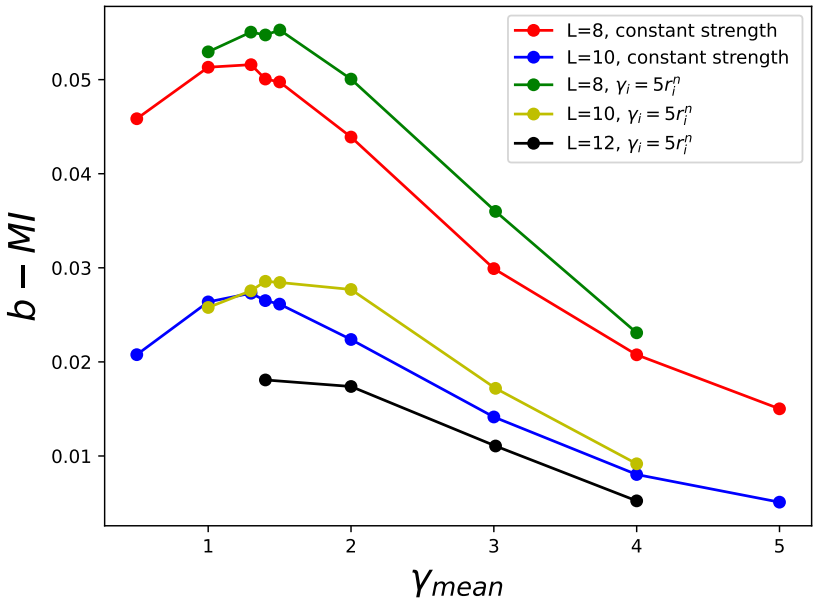

(a) Bipartite mutual information

Figure 4.10: Comparison of Bipartite Mutual Information for Constant (labelled as uniform) and $5r^n$ distributions of measurement strengths.

If we observe the Fig. 4.10a, by considering both lengths $L = 8$ and 10 we see that the peak of bipartite Mutual Information occurs at around $\gamma_{mean} = 1.3$ for constant

measurements strengths and at $\gamma_{mean} = 1.4$ for the distribution $5r^n$. As we increase the size of the system the estimation of the exact position of peak gets better. Thus the critical measurement strength for the distribution $5r^n$ can be said to be around $\gamma_{mean} = 1.4$ if the transition happens in this system.

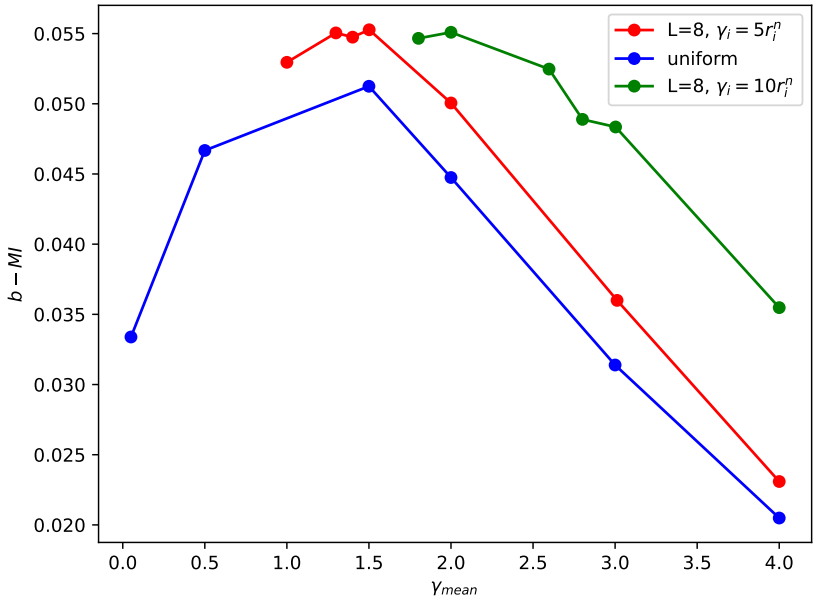

(a) b-MI

Figure 4.11: Comparison of bipartite mutual information for constant and $10r^n$ distributions of measurement strengths.

When we observe Fig. 4.11a we find that the peak of bipartite mutual information is shifted forward for the distribution $10r^n$. The value of peak can be estimated to be around $\gamma_{mean} = 2$ which is more than that of $5r^n$ distribution. This value can change slightly when we take larger system sizes into consideration. Also, we observe that the more the γ_{max} of the distribution, the higher the values of bipartite mutual information will be than the constant case.

For the tripartite mutual information (t-MI) Fig. 4.12a we observe that as the length increases the absolute values of t-MI decrease. These values are greater than their constant case counterparts.

For the tripartite mutual information (t-MI) Fig. 4.13a we observe that when we increase the γ_{max}, the absolute values of t-MI increases. There is a considerably greater increase from the $5r^n$ distribution values to $10r^n$ distribution values than from constant to $5r^n$ at least in the $L = 8$ case.

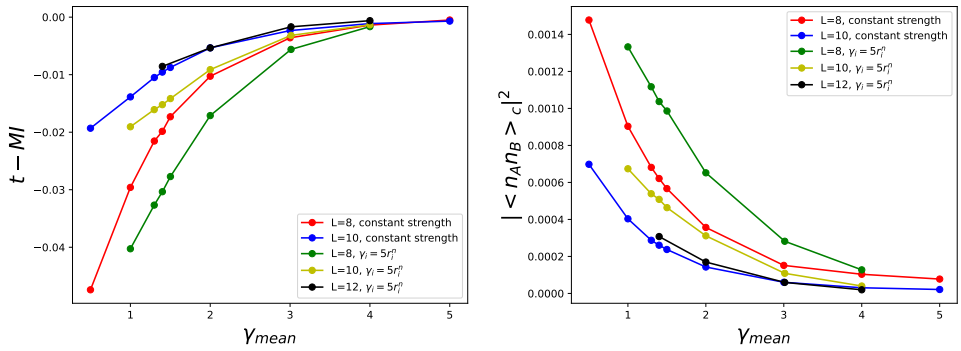

(a) t-MI **(b)** nn correlation

Figure 4.12: Comparison of t-MI and connected correlation function of constant and $5r^n$ distributions.

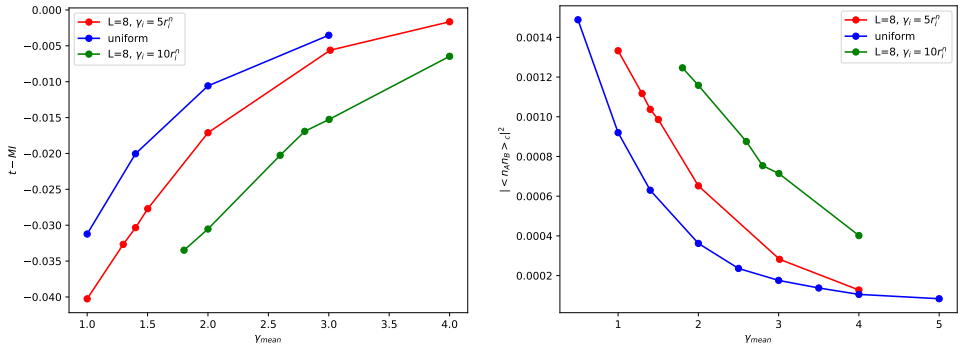

(a) t-MI **(b)** nn correlation

Figure 4.13: Comparison of t-MI and connected correlation function of constant, $5r^n$ and $10r^n$ distributions.

In the connected correlation function of the number operator, the values for $5r^n$ and $10r^n$ distribution are greater than the constant case and the increase is greater with the value of γ_{max}.

4.2.4. Probability distribution of Single-Site entropy for boson chain with $V = 0$

Here we study the probability distribution of single-site von Neumann entanglement entropy for distributions $5r^n$ and $10r^n$. For easy comparison, we have also plotted the same for the constant case described in Chapter 3 alongside it.

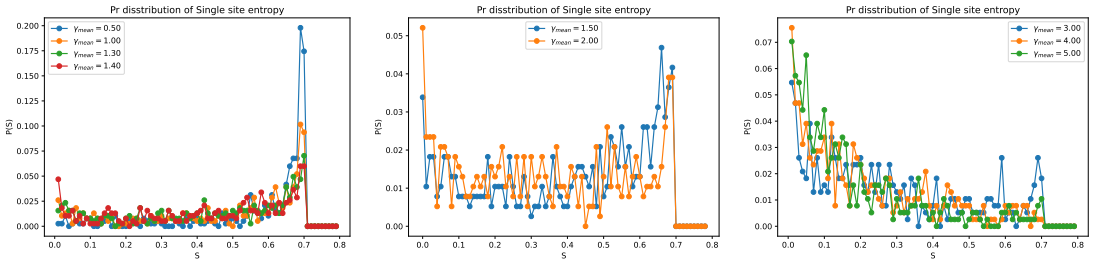

(a) L=8 **(b)** L=8 **(c)** L=8

Figure 4.14: Probability distribution of Single-Site entropy for constant strengths

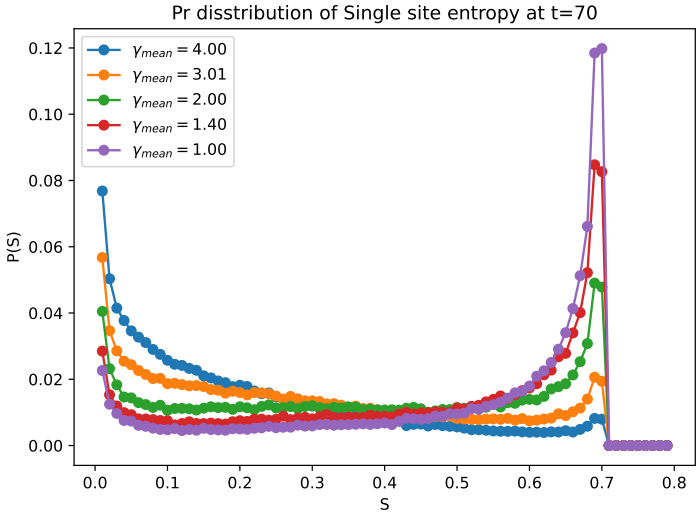

(a) Probability distribution of Single-Site entropy for $5r^n$, $L = 8$

As previously observed in the constant strength case here also different probability distributions of single-site entropy are obtained for smaller and larger values of measurement strengths. We observe that for $L = 8$ and $5r^n$ distribution Fig. 4.15a,

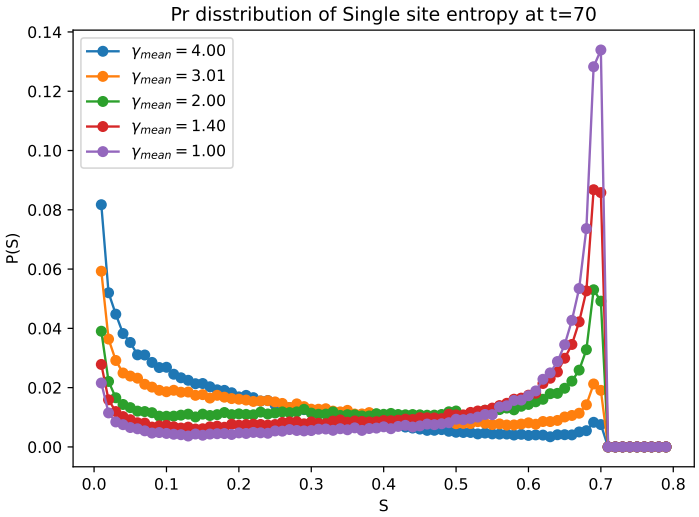

(a) Probability distribution of Single-Site entropy for $5r^n$, $L = 10$

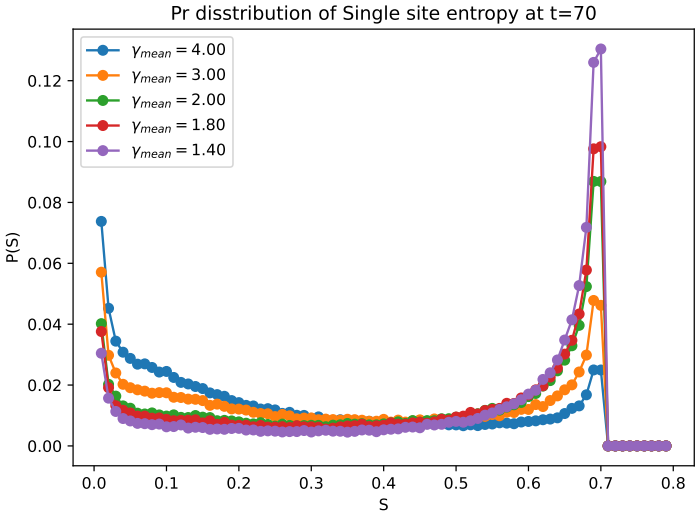

(a) L=8, $10r^n$

Figure 4.17: Probability distribution of Single-Site entropy for $10r^n$

almost equal heights of peaks are present in the region near $S = 0$ and $S > 0$ for $\gamma_{mean} = 2$. (We have named the far right end of the plot as $S > 0$ region and the far left end as $S = 0$ region.) Values for $\gamma_{mean} = 4$ and $\gamma_{mean} = 3$ have sharper peaks around $S = 0$. On the other hand probability distribution for $\gamma_{mean} = 1$ has a sharp peak in the $S > 0$ region, which starts decreasing as the value of γ_{mean} increases. Similar trends are observed for the $L = 10$ case for this distribution Fig. 4.16a.

For $L = 8$ and $10r^n$ distribution Fig.4.17 the values of peaks at S>0 region are sharper for $\gamma_{mean} = 1.4$, $\gamma_{mean} = 1.8$ and $\gamma_{mean} = 2$. The peaks for $\gamma_{mean} = 3$ and $\gamma_{mean} = 4$ are higher in the $S = 0$ region though the difference between these peaks is lesser than that of their counterparts in the $5r^n$ case, meaning they are not as deep in the low entanglement regime as in the previous case. This matches with our observation from the peak of bipartite mutual function, that the measurement-induced critical point can shift forward as the value of γ_{max} is increased.

When compared with the constant strengths case probability distribution of single-site entropy, the plots for the random strengths are smoother as there was an overall greater number of single-site entropy values for the random case, as the number of runs itself was larger than the constant case.

4.2.5. Time evolution of different trajectories and realizations for boson chain with $V = 0$

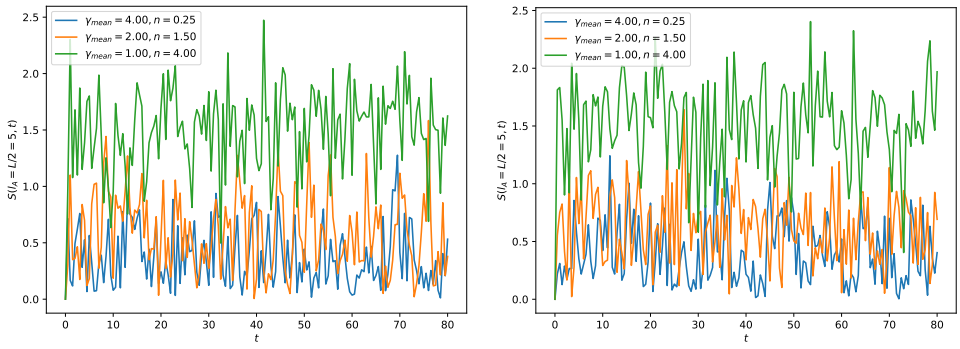

(a) trajectory 0 **(b)** trajectory 8

Figure 4.18: Entanglement entropy

In Fig. 4.18 we have shown the evolution of entanglement entropy values and in fig. 4.19 we have shown time evolution of tripartite mutual information for trajectories

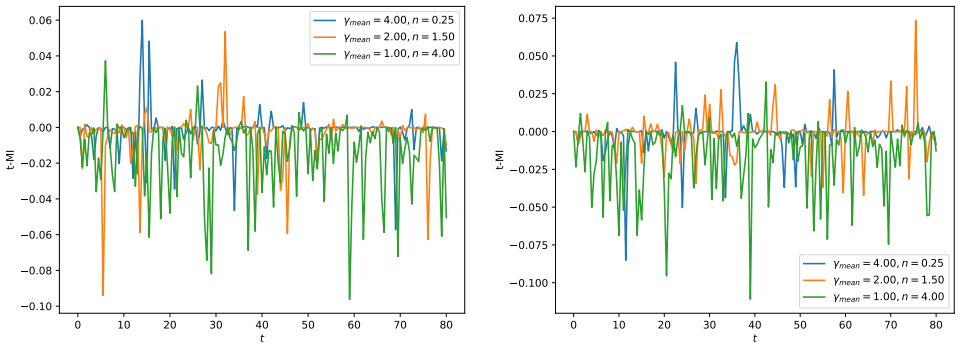

(a) trajectory 0 **(b)** trajectory 8

Figure 4.19: tripartite mutual information

numbered 0 and 8 for the same realization numbered 0. The difference in the fluctuations is because of the different random numbers chosen in different trajectories.

4.2.6. Steady state entanglement entropy for interacting boson chain

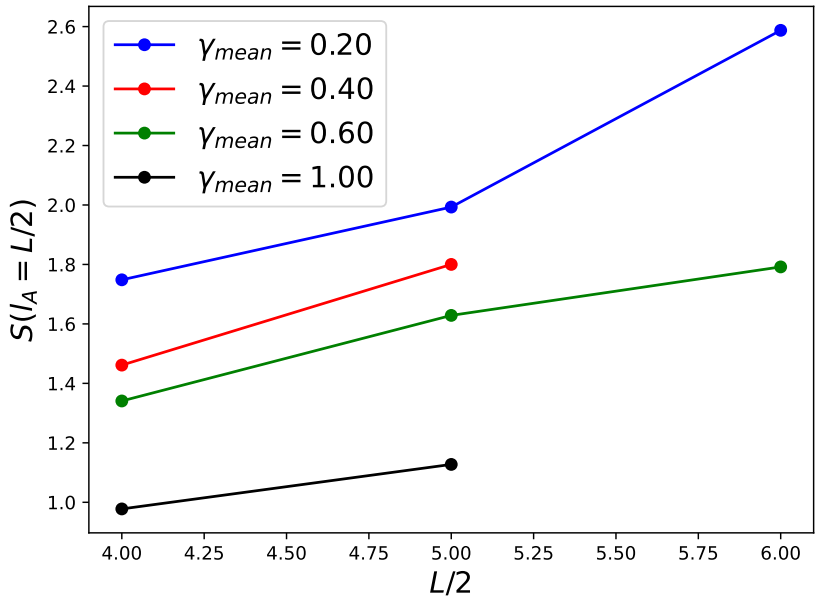

(a)

Figure 4.20: Steady state entanglement entropies plotted against half of the system size L for different strengths γ_{mean}. Averages are taken over the interval 50-80. $V = 1, J' = 0, J = 1$

An increase in the half-chain entanglement entropy is seen with increasing the values of the system size.

4.2.7. Mutual information and correlation function for interacting boson chain

Here we study the interacting case for the hard-core boson chain with continuous measurements. For taking the following data we have used $V = 1, J = 1$ and $J' = 0$ with half-filling. Again we use two distributions $5r^n$ and $10r^n$ and compare them with the constant measurement strengths case. The data is averaged over time window $50 < t < 80$ and $dt = 0.01$. Quantities are calculated at every 50th step.

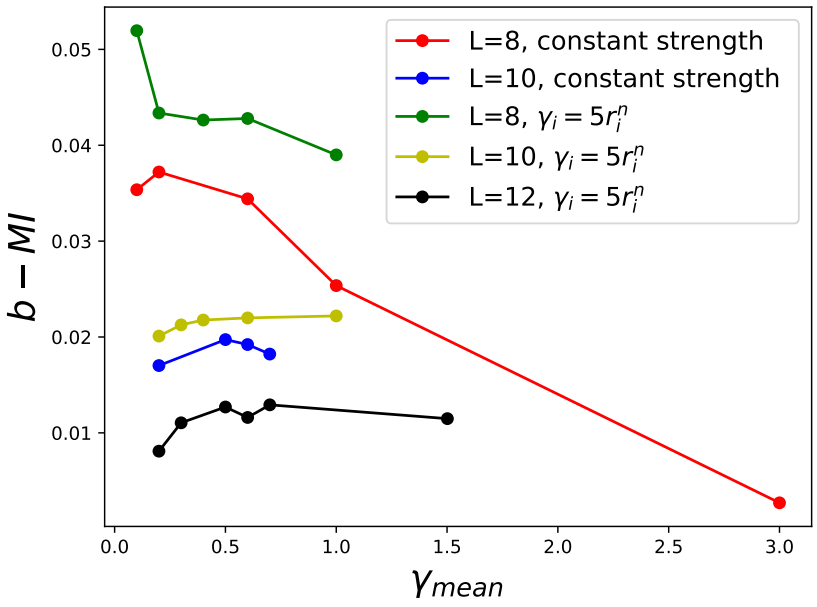

(a) Bipartite mutual information

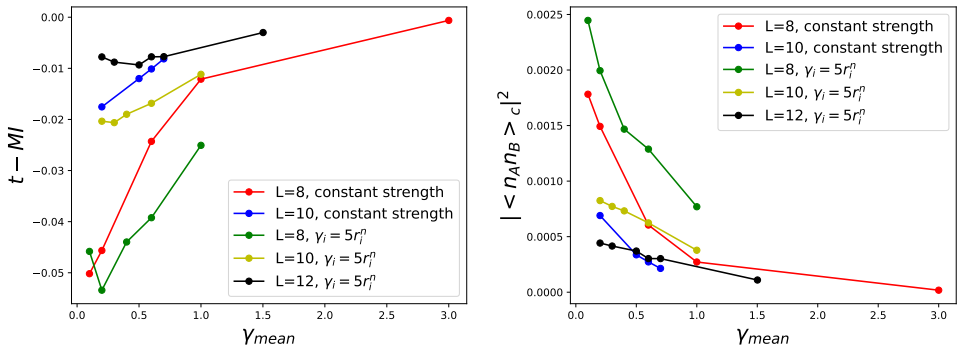

(a) t-MI **(b)** nn correlation

Figure 4.22: $5r^n$ and constant comparison for $V = 1, J' = 0$

Bipartite mutual information

In the constant measurement strengths case of interacting hard-core boson chain,

the peak of the bipartite mutual information for the $L = 10$ system is around the γ_{mean} value of 0.5 (Fig. 4.21a).

The bipartite mutual information for the $5r^n$ distribution has no clear peak at least with the amount of data obtained, though values of bipartite mutual information show an initial increase with γ_{mean} (Fig. 4.21a).

As observed in the non-interacting case, the values of bipartite mutual information for $5r^n$ are greater than that of the constant measurement case, though the increase is higher for $L = 8$ size than that of $L = 10$. Previously in the non-interacting case, the increase for both system sizes was roughly similar.

We have also plotted these values for the distribution $10r^n$ distribution, for system size $L = 8$ in comparison to those with $5r^n$ and constant strengths case (4.23).

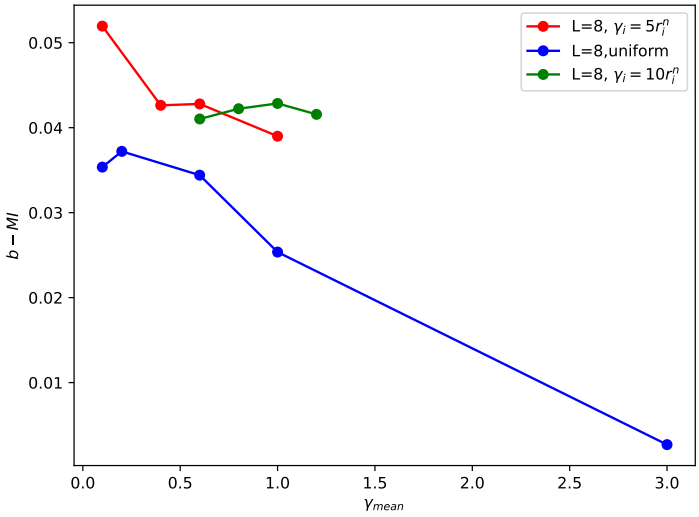

(a) b-MI

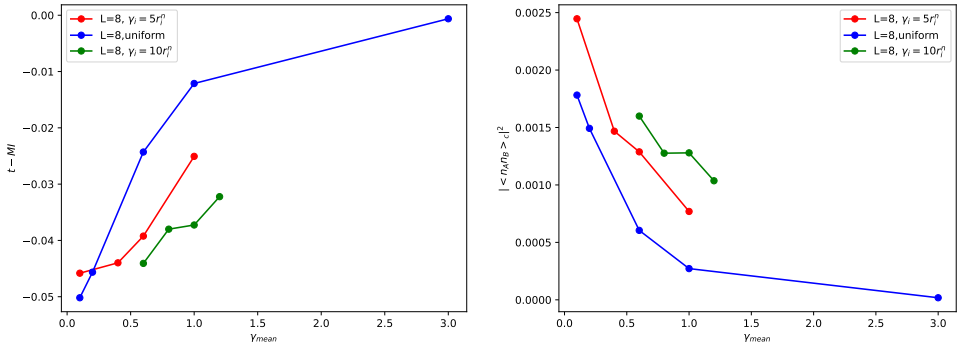

(b) t-MI

(c) nn correlation

Figure 4.23: $5r^n$, $10r^n$ and constant comparison for $V = 1, J' = 0$

Tripartite mutual information

As in the previous case of the non-interacting chain, the absolute values of tripartite mutual information for this distribution are greater than that of the case of the constant strengths. They increase with increasing γ_{max}. The exact values start approaching zero from the negative end as the γ_{mean} increases. (see Fig. 4.22a and Fig. 4.23b).

Connected correlation function

The values of the connected correlation function are higher than their constant case counterparts and increase with increasing γ_{max} (see Fig. 4.22b and Fig. 4.23c).

4.2.8. Probability distribution of single site entanglement entropy for interacting chain

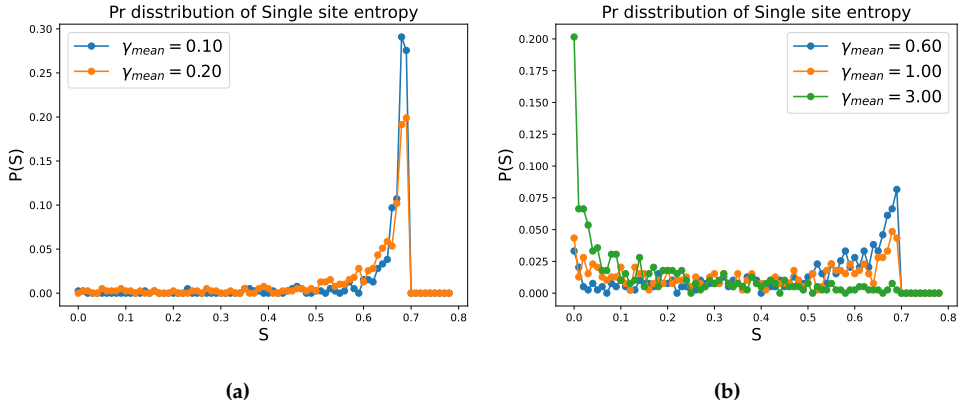

(a) (b)

Figure 4.24: Probability distribution of entanglement entropy for $L = 8, V = 1, J' = 0$ for constant measurement strengths.

From the probability distribution of single-site entanglement entropy, we can see very sharp peaks for γ_{mean} values 0.1 and 0.2 in the $S > 0$ region. In fact, there is no peak in the $S = 0$ region. (see Fig. 4.24a)

Around $\gamma_{mean} = 0.6$ and $\gamma_{mean} = 1$ the peaks at $S > 0$ region start decreasing and peaks near the $S = 0$ region appear. Their heights are also almost the same (more similar for $\gamma_{mean} = 1$). For $\gamma_{mean} = 3$ there is only one peak in the S=0 region and no peak in the S>0 region. (see Fig. 4.24b)

A similar trend is observed for the $L = 8, 5r^n$ case. For γ_{mean} values 0.1 and 0.2, sharp peaks are present in $S > 0$ region and no peak at $S = 0$ region (see Fig. 4.25a).

We have also plotted the values for $L = 8, 10r^n$ (Fig.4.25b) case and $L = 12, 5r^n$ case (Fig.4.26). The position of the peaks of probability distribution gives us an idea as to

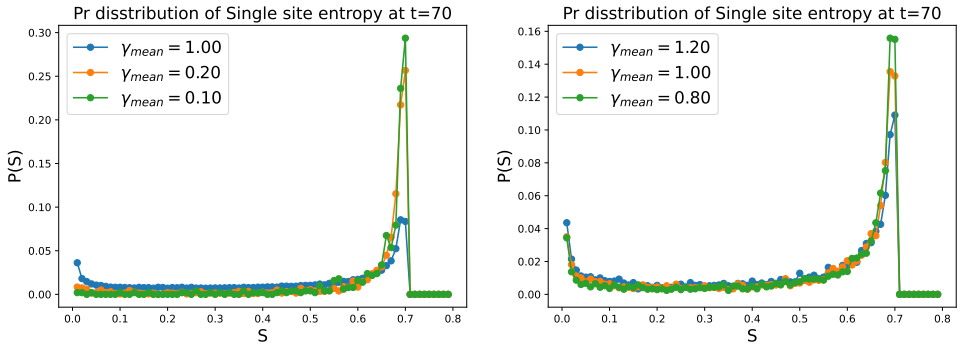

(a) $L = 8, 5r^n$ **(b)** $L = 8, 10r^n$

whether the γ_{mean} values lie in volume or area law phase if these phases are present.

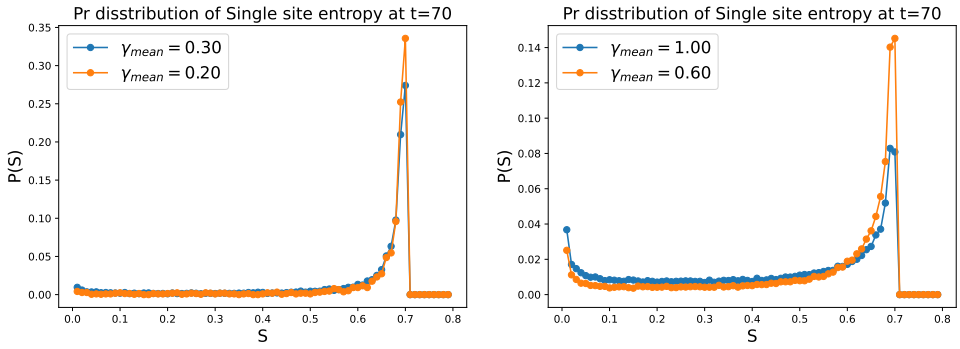

(a) **(b)**

Figure 4.26: Probability distribution of entanglement entropy for $L = 10, V = 1, J' = 0$ for $5r^n$.

5

Finite Size Scaling at Entanglement transitions

We can approximate the value of γ_c where the entanglement transition takes place from the peak positions of bipartite mutual information if a signature of transition is present in the entanglement profiles of the system.

5.1. Scaling Behaviours at Entanglement transitions

As per Ref. [10], the von Neumann entanglement entropy under periodic boundary conditions of a 1D critical system is given by,

$$S(l_A) = \frac{c}{3} ln x_A + c' \tag{5.1}$$

where x_A is called the chord length of subsystem A, c is the central charge and c' is a non-universal constant.

$$x_A = \frac{L}{\pi} sin(\frac{\pi l_A}{L}) \tag{5.2}$$

Thus, the scaling form at the entanglement transition can be written as,

$$S(l_A) = \alpha_S ln x_A + \beta_S \tag{5.3}$$

Steady-state values of the entanglement entropies for constant measurement strengths case with $V = 0, J' = 1, J = 1$, for different subsystem sizes at entanglement transition are shown in Fig. 5.1a and fitted with this scaling form (Eq. 5.3).

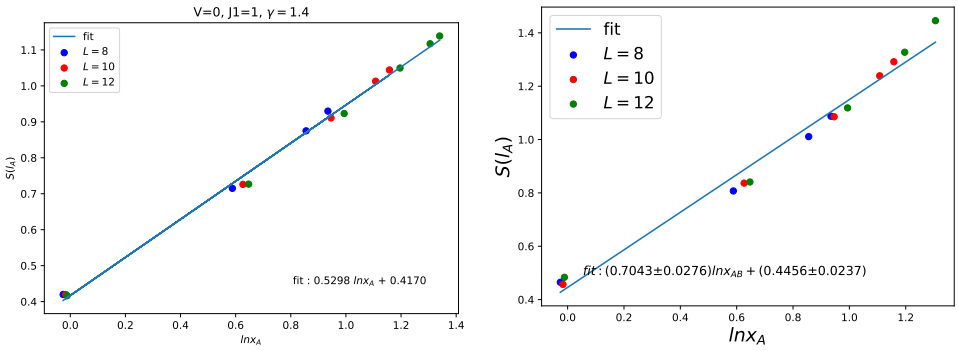

(a) constant measurement strengths case, $\gamma = 1.4$ **(b)** $5r^n$ distribution, $\gamma = 1.4$

Figure 5.1: Scaling of Entanglement entropy for non-interacting ($V = 0, J' = 1$), for constant and $5r^n$ distributions for $\gamma_{mean} = 1.4$.

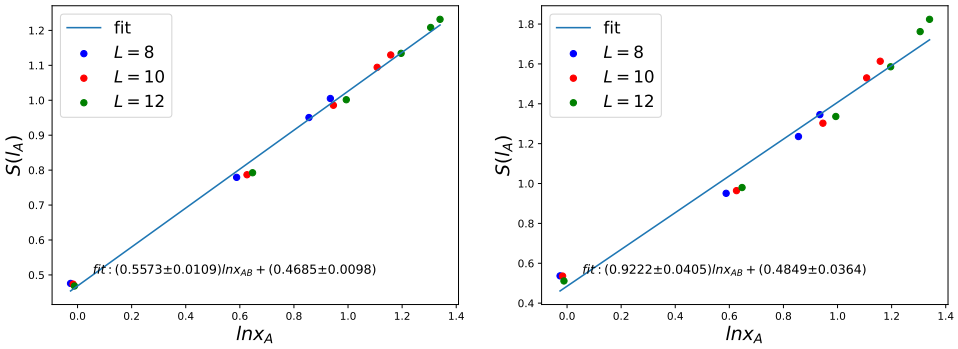

(a) constant measurement strengths case **(b)** $5r^n$ distribution

Figure 5.2: Scaling of Entanglement entropy for interacting ($V = 1, J' = 0$), for constant and $5r^n$ distributions for $\gamma_{mean} = 0.6$.

Value of α_S for $V = 0, J' = 1$ case with constant measurement $\longrightarrow$ 0.5298

The value of α_S for $V = 0, J' = 1$ case in the paper [10] with constant measurement is about 0.526. In that paper they have gone till $L = 20$ system sizes.

Thus the value of the central charge c is thus, 1.5894.

Value of β_S for $V = 0, J' = 1$ case with constant measurement $\longrightarrow$ 0.4170

The values of central charge and α are summarized in the table no. 5.1 below.

Collapse

Around the transition $\gamma \sim \gamma_c$, the entanglement entropy is proposed to follow the scaling form,

$$S(\gamma, L; l_A = aL) - S(\gamma_c, L; l_A = aL) = F[(\gamma - \gamma_c)L^{1/\nu}] \tag{5.4}$$

here, we select $a = 1/2$ and F is a smooth function.

The divergence of correlation length is $\xi \sim |\gamma - \gamma_c|^{-\nu}$ at the MIC.

1. Estimate critical points γ_c from peak structures of the mutual information

2. Perform the scaling analysis for data sets in the range $\gamma \in [\gamma_c - 1, \gamma_c + 1]$ and for $L = 8$ to 12.

The entanglement entropy shows finite size dependence near the critical transition point. We try to find the optimized exponent ν, such that the data for S for all γ values in the range and all L collapse into a single curve given by the Eq. 5.4. We can do this by minimizing the χ^2-function in multi-parameter space [18], defined as,

$$\chi^2(\{c_k\}; \{d_k\}) = \sum_{L,\gamma} [S(\gamma, L) - F[(\gamma - \gamma_c)L^{1/\nu}]]^2 \tag{5.5}$$

where $S(\gamma, L)$ are the data points at different values of γ and L.

We take F to be described by $c_0 + c_1 x + c_2 x^2$ where c_0, c_1, c_2 are obtained from the minimization process. x here is equal to $(\gamma - \gamma_c)L^{1/\nu}$.

We have performed scaling collapse for the constant measurement strengths case with $V = 0, J' = 1$ (Fig. 5.4a) with the value of $\nu = 1.201395$ and for random measurement strengths case with $V = 0, J' = 1$ (Fig. 5.4a) with the value of $\nu = 1.201390$ obtained by minimizing χ^2. The minimized value of χ^2 is 0.00455 for constant case.

The value of ν obtained in the paper [10] is 1.22 for constant case.

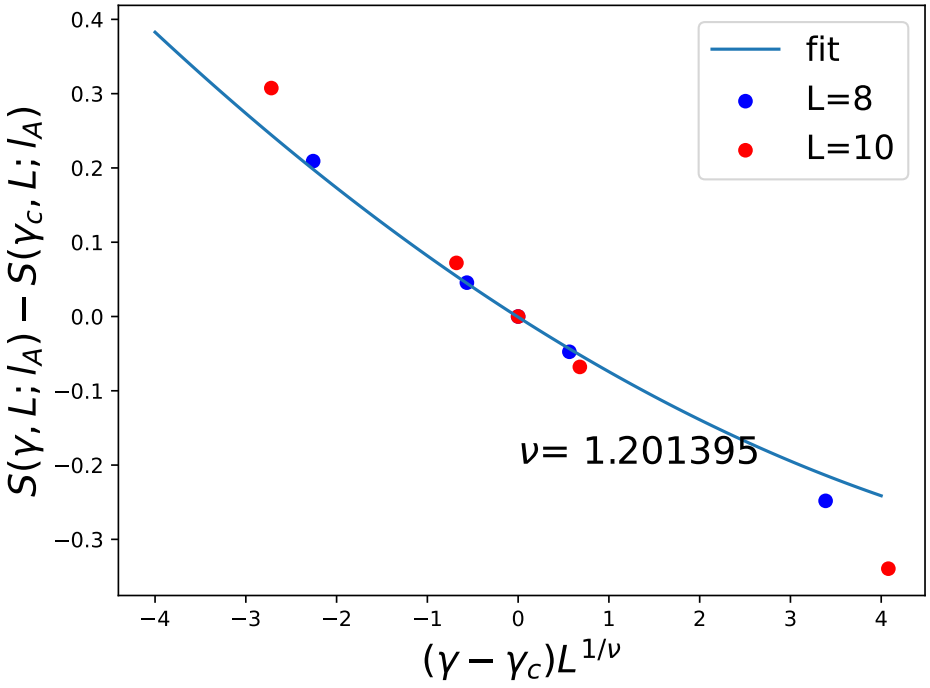

(a) $V = 0, J' = 1$ for constant measurement strengths case, $\gamma_c = 1.4$

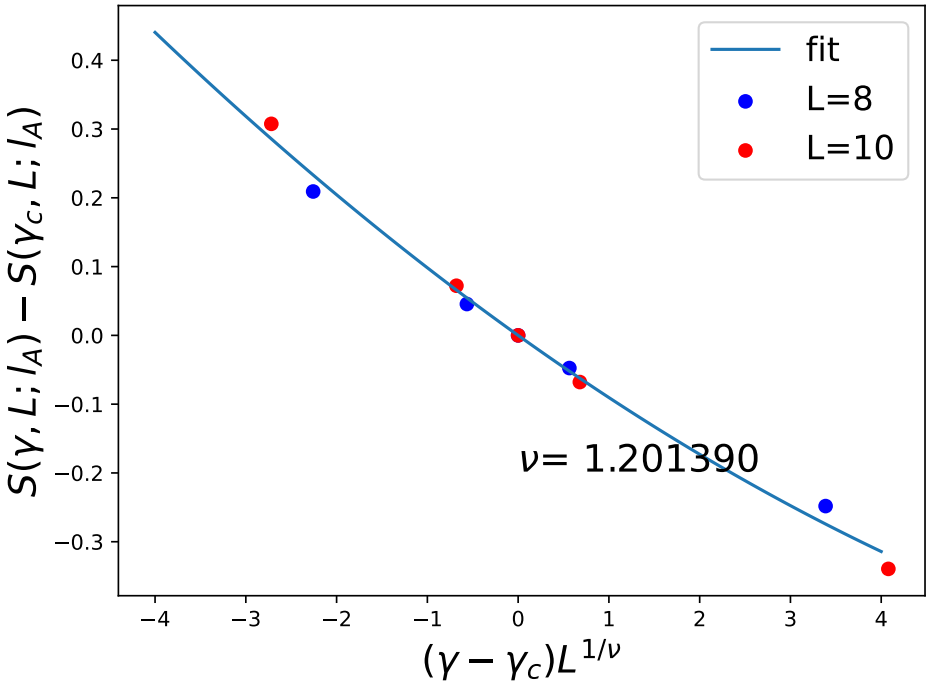

(a) $V = 0, J' = 1$ for random measurement strengths case with $\gamma_{max} = 5$, $\gamma_c = 1.4$.

5.2. Scaling behaviour of bipartite mutual information

We will study the scaling behaviour of $I_{AB}(r_{AB})$ as a function of the distance r_{AB} between two sites at $\gamma = \gamma_c$. Scaling is done for values in the steady-state regime.

Power-law behaviours $I_{AB} \propto x_{AB}^{-2\Delta}$ for large distances are present. [10]

We have plotted $ln(b-MI)$ against lnx_{AB} for various distributions for non-interacting and interacting cases.

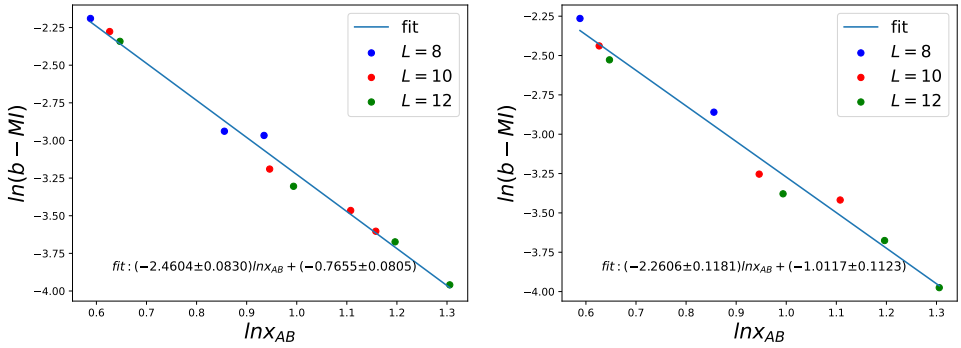

(a) constant measurement strengths case, $\gamma = 1.4$ **(b)** $5r^n$ distribution, $\gamma = 1.4$

Figure 5.5: Scaling of bipartite mutual information for non-interacting ($V = 0, J' = 1$), for constant and $5r^n$ distributions for $\gamma_{mean} = 1.4$.

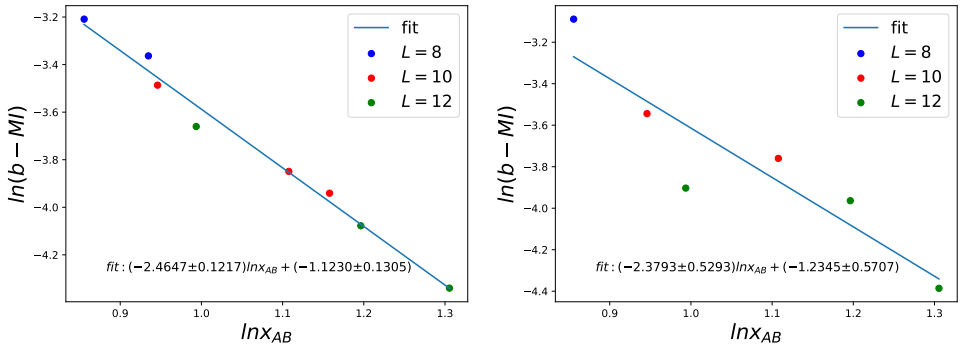

(a) constant measurement strengths case **(b)** $5r^n$ distribution

Figure 5.6: Scaling of bipartite mutual information for interacting ($V = 1, J' = 0$), for constant and $5r^n$ distributions for $\gamma_{mean} = 0.6$.

For $\gamma = 1.4, V = 0$ constant distribution case, the fit is obtained and the slope value is -2.4604.

Thus, $I_{AB} \propto x_{AB}^{-2.4604}$. From this, we obtain the value of $\Delta = 1.2302$

Values of Δ for other distributions are given in the table below.

values/Model	C : (V,J')= (0,1)	R :(V,J')= (0,1)	C :(V,J')= (1,0)	R : (V,J')= (1,0)
α_S	0.5298	0.7043	0.5573	0.9222
c	1.5894	2.1129	1.6719	2.7666
Δ	1.2302	1.1303	1.2323	1.1896

Table 5.1: C represents constant measurement strengths case and R represents random measurement strengths case with $\gamma_{max} = 5$

5.3. Scaling behaviour of correlation function

We will study the scaling behaviour of the correlation function as a function of chord distance x_{AB}.

Power law behaviour of the form $| < n_1 n_{r_{AB}+1} >_c |^2 \propto x_{AB}^{-2\Delta_n}$ is observed.

We follow the same method as done for the scaling of bipartite mutual information, but fitting is done only for values with $lnx_{AB} > 1$. [10]

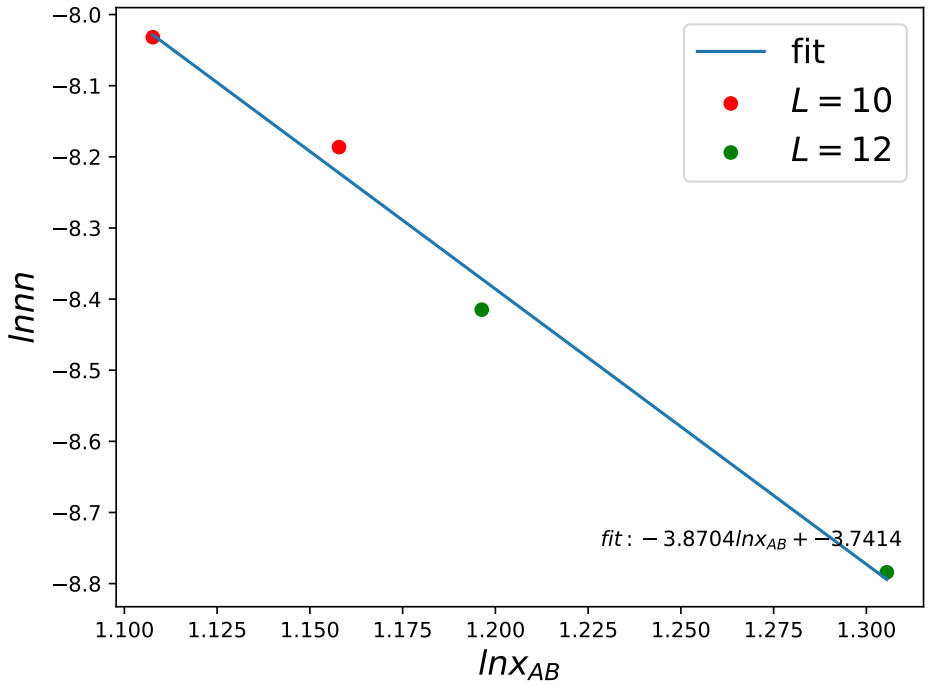

Thus we obtain the value of $\Delta_n = \frac{3.8704}{2} = 1.9352$

The value of Δ_n is larger than those of Δ obtained for the mutual information. This could be because the functional forms of this nn correlation function in γ do not follow that of mutual information.[10]

We have compared the values of the exponents in the table below,

We need to note that the values of α, Δ and Δ_n were obtained only considering system sizes 8, 10 and 12. They can get better by considering more systems with larger sizes.

6

Conclusion and Outlook

For the non-interacting boson chain under measurement with random strengths selected from a uniform distribution, we got changes in the values of steady-state entanglement entropy with increasing variances. Though as these variances are not comparable with the values of γ_{mean} only a slight increase is observed.

Under the random measurement strengths selected from $\gamma_{max} r_i^n$ distribution, for the non-interacting case with $\gamma_{max} = 5$, we observe linear growth in half-chain entanglement entropy for smaller values of γ_{mean} and the increased is suppressed for larger γ_{mean}. This suggests a possible entanglement transition, which can be compared with the peak of bipartite mutual information occurring at the γ_{mean} value 1.4. With increasing γ_{max} to 10 we observe a forward shift in this peak's position.

More results for higher system sizes and various γ_{mean} values are required for the interacting boson chain to conclusively observe entanglement transition if it is present. We have obtained ν right now only for constant non-interacting case. With more values of γ_{mean} and lengths, we will also perform scaling collapse for the other cases.

The non-interacting hard-core boson chain Hamiltonian with V=0 can be mapped to one particle fermionic system Hamiltonian H_f and equivalently becomes a spin-1/2 fermionic chain. As the matrix of this H_f has fewer entries, it becomes easy to reach larger system sizes using numerical calculations in a shorter time span than using a bosonic system. This can be solved by more efficient numerical evolution using QR decomposition of the time evolution operator. Thus we can check if the transition

happens at larger system sizes in future work.

References

[1] Exact diagonalization studies, Anders W. Sandvik.

[2] Rajeev Acharya et al. "Suppressing quantum errors by scaling a surface code logical qubit". In: *Nature* 614 (2022), pp. 676–681. URL: https://api.semanticscholar.org/CorpusID:250526184.

[3] Niels Henrik David Bohr. "The Quantum Postulate and the Recent Development of Atomic Theory". In: *Nature* 121 (1928), pp. 580–590. URL: https://api.semanticscholar.org/CorpusID:4097746.

[4] Heinz-Peter Breuer and Francesco Petruccione. *The Theory of Open Quantum Systems*. Oxford University Press, Jan. 2007. ISBN: 9780199213900. DOI: 10.1093/acprof:oso/9780199213900.001.0001. URL: https://doi.org/10.1093/acprof:oso/9780199213900.001.0001.

[5] Amos Chan et al. "Unitary-projective entanglement dynamics". In: *Phys. Rev. B* 99 (22 June 2019), p. 224307. DOI: 10.1103/PhysRevB.99.224307. URL: https://link.aps.org/doi/10.1103/PhysRevB.99.224307.

[6] Andrew Daley. "Quantum trajectories and open many-body quantum systems". In: *Advances in Physics* 63 (May 2014). DOI: 10.1080/00018732.2014.933502.

[7] J. M. Deutsch. "Quantum statistical mechanics in a closed system". In: *Phys. Rev. A* 43 (4 Feb. 1991), pp. 2046–2049. DOI: 10.1103/PhysRevA.43.2046. URL: https://link.aps.org/doi/10.1103/PhysRevA.43.2046.

[8] Laird Egan et al. "Fault-tolerant control of an error-corrected qubit". In: *Nature* 598 (2021), pp. 281–286. URL: https://api.semanticscholar.org/CorpusID:238357892.

[9] Richard Phillips Feynman and Frank L. Vernon. "The Theory of a general quantum system interacting with a linear dissipative system". In: *Annals of Physics* 24 (1963), pp. 547–607. URL: https://api.semanticscholar.org/CorpusID:207506984.

[10] Yohei Fuji and Yuto Ashida. "Measurement-induced quantum criticality under continuous monitoring". In: *Physical Review B* 102 (Aug. 2020). DOI: 10.1103/PhysRevB.102.054302.

[11] Matteo Ippoliti et al. "Entanglement Phase Transitions in Measurement-Only Dynamics". In: *Phys. Rev. X* 11 (1 Feb. 2021), p. 011030. DOI: 10.1103/PhysRevX.11.011030. URL: https://link.aps.org/doi/10.1103/PhysRevX.11.011030.

[12] Kurt Jacobs and Daniel Steck. "A Straightforward Introduction to Continuous Quantum Measurement". In: *Contemporary Physics* 47 (Nov. 2006). DOI: 10.1080/00107510601101934.

[13] Sebastian Krinner et al. "Realizing repeated quantum error correction in a distance-three surface code". In: *Nature* 605.7911 (May 2022), pp. 669–674. ISSN: 1476-4687. DOI: 10.1038/s41586-022-04566-8. URL: http://dx.doi.org/10.1038/s41586-022-04566-8.

[14] David Lanlege et al. "Comparison of Euler and Range-Kutta methods in solving ordinary differential equations of order two and four". In: (June 2018), pp. 10–37.

[15] Yaodong Li, Xiao Chen, and Matthew P. A. Fisher. "Measurement-driven entanglement transition in hybrid quantum circuits". In: *Phys. Rev. B* 100 (13 Oct. 2019), p. 134306. DOI: 10.1103/PhysRevB.100.134306. URL: https://link.aps.org/doi/10.1103/PhysRevB.100.134306.

[16] Yaodong Li, Xiao Chen, and Matthew P. A. Fisher. "Quantum Zeno effect and the many-body entanglement transition". In: *Phys. Rev. B* 98 (20 Nov. 2018), p. 205136. DOI: 10.1103/PhysRevB.98.205136. URL: https://link.aps.org/doi/10.1103/PhysRevB.98.205136.

[17] Giulia Piccitto, Angelo Russomanno, and Davide Rossini. "Erratum: Entanglement transitions in the quantum Ising chain: A comparison between different unravelings of the same Lindbladian [Phys. Rev. B 105, 064305 (2022)]". In: *Phys. Rev. B* 106 (21 Dec. 2022), p. 219901. DOI: 10.1103/PhysRevB.106.219901. URL: https://link.aps.org/doi/10.1103/PhysRevB.106.219901.

[18] Sibaram Ruidas and Sumilan Banerjee. "Semiclassical Limit of a Measurement-Induced Transition in Many-Body Chaos in Integrable and Nonintegrable Oscillator Chains". In: *Physical Review Letters* 132.3 (Jan. 2024). ISSN: 1079-7114.

DOI: 10.1103/physrevlett.132.030402. URL: http://dx.doi.org/10.1103/PhysRevLett.132.030402.

[19] Brian Skinner, Jonathan Ruhman, and Adam Nahum. "Measurement-Induced Phase Transitions in the Dynamics of Entanglement". In: *Phys. Rev. X* 9 (3 July 2019), p. 031009. DOI: 10.1103/PhysRevX.9.031009. URL: https://link.aps.org/doi/10.1103/PhysRevX.9.031009.

[20] Qicheng Tang and W. Zhu. "Measurement-induced phase transition: A case study in the nonintegrable model by density-matrix renormalization group calculations". In: *Physical Review Research* 2 (Jan. 2020). DOI: 10.1103/PhysRevResearch.2.013022.

[21] Howard M. Wiseman and Gerard J. Milburn. *Quantum Measurement and Control*. Cambridge University Press, 2009.

[22] Kazuki Yamamoto and Ryusuke Hamazaki. "Localization properties in disordered quantum many-body dynamics under continuous measurement". In: *Phys. Rev. B* 107 (22 June 2023), p. L220201. DOI: 10.1103/PhysRevB.107.L220201. URL: https://link.aps.org/doi/10.1103/PhysRevB.107.L220201.

[23] Aidan Zabalo et al. "Infinite-randomness criticality in monitored quantum dynamics with static disorder". In: *Physical Review B* 107 (June 2023). DOI: 10.1103/PhysRevB.107.L220204.

[24] Wojciech Hubert Zurek. "Decoherence, einselection, and the quantum origins of the classical". In: *Rev. Mod. Phys.* 75 (3 May 2003), pp. 715–775. DOI: 10.1103/RevModPhys.75.715. URL: https://link.aps.org/doi/10.1103/RevModPhys.75.715.